Università di Roma Tor Vergata

Corso di Laurea Magistrale in Physics of Complex Systems and Big Data

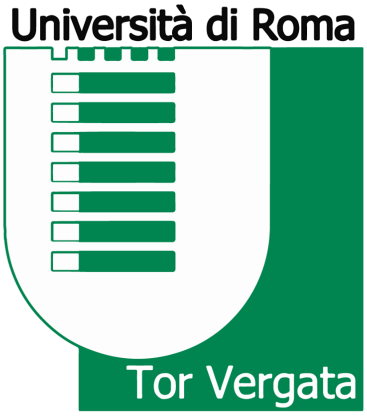

Electron-phonon coupling in semiconductors by finite difference displacements

Candidato:

Pierre Lechifflart

Relatori:

Maurizia Palummo

Claudio Attaccalite

Correlatore:

Olivia Pulci

Sessione di laurea 23 Ottobre 2020

A.A. 2019/2020

Contents

Introduction

Thermal effects on the electronic band structure of solids due to electron-phonon interactions have been explored in the 1980's by Manuel Cardona *et al.* from both the experimental and theoretical sides using a perturbative approach in the electron-phonon interaction [1, 2].

This approach has been then extended to include dynamical effects [3, 4], more efficient sampling techniques [5, 6] and applied in the study of carrier lifetime, mobility, transport, kinks and satellites (for a review see Ref. [7]). Simultaneously with these perturbative approaches a new way to evaluate thermal effects emerged in the scientific literature : the use of finite difference displacements (FDD). Numerous efficient sampling techniques have been proposed in the literature [8, 9, 10] that allow a systematic study of electronic properties at finite temperature.

These methods have two main advantages. First they are much more efficient than standard classical or path-integral molecular dynamics [11]. Second, finite difference displacements allow the calculation of thermal effects on observables that are difficult to treat within the perturbative approaches as for instance topological observables [12], nuclear magnetic response [13] or x-ray absorption near-edge structures [14]. For example, thank to the FDD approach it was possible to investigate the correlations effects on electron-phonon coupling in bulk materials [15, 16] and finite systems [17].

The disadvantage of these approaches is that they require large supercells for the calculations to converge, and do not allow the inclusion of dynamical effects [4]. In this work we apply the finite difference displacements[10] to study thermal effects on the electronic band gap of three systems : polyethylene, hexagonal Boron Nitride and Phosphorene. These materials have been chosen for different reasons: polyethylene is a one dimensional chain, and therefore we expect easier convergence, from the point of view of the computational cost, with the cell size; boron-nitride is a simple system with a strong electron-phonon coupling; and finally phosphorene has the advantage to

not be a polar materials and therefore electron-phonon coupling does not include long range terms. Thermal effects on the band gap have been studied since the 1950's, and recently it has also been shown that many-body corrections to the band structure can strongly renormalize the electron-phonon coupling, but little is known about the thermal effects on other electronic properties. In monolayer black phosphorus, also known as Phoshorene, experimental measurements show that the electron-hole pairs do not follow usual theoretical predictions [18] but have their behaviors modified by temperature [19]. Part of this behaviour may originate from the single-particle band structure due to the interplay between thermal expansion and electron-phonon coupling [20] or due to correlation effects [16]. But without a precise calculation it is very difficult to differentiate these effects from thermal behavior of the electron-hole pair binding energy. For this reason we decide to investigate the electron-phonon coupling of Phosphorene by using finite difference displacement method that is easy to implement and to control.

Several methods for optimizing both the computational time and accuracy of finite differences displacements methods have been proposed. In this work we focus in particular on the methods proposed by Monserrat [8] and by Zacharias and Giustino [10]. In this work we tested both of these and choose the best-suited method for our purpose. The final goal of this work is the understanding of the anomalous behavior of optical properties with the temperature in bulk materials by means of a new theoretical approach. However, for the moment in this work, we concentrate on the electronic band structure only, leaving the optical properties for further work. The thesis is so organized: in chapter one we present the theoretical framework used for the electronic structure calculations; in chapter two we present the theory of phonon and electron-phonon coupling by finite differences, and finally in chapter three we present the results and draw the conclusions.

Chapter 1

Theoretical framework

Modern problems in solid state physics include systems with dozens of atoms or more. Take a macroscopic crystal, it contains in the order of 10^{23} atoms. Each atom having three degrees of freedom , we are left with a computationally intractable problem. Therefore one need use multiple approximations to solve many-body problems.

1.1 Born-Oppenheimer approximation

The first approximation commonly used is the Born-Oppenheimer approximation. Given a system of N similar interacting atoms, its (non relativistic and time-independent) Hamiltonian writes :

$$\begin{aligned}\mathcal{H} = &-\sum_I \frac{\hbar^2}{2M_I}\boldsymbol{\nabla}_I^2 - \frac{\hbar^2}{2m_e}\sum_i \boldsymbol{\nabla}_i^2 \\ &+ \frac{1}{2}\sum_{I\neq J}\frac{Z_I Z_J e^2}{|\mathbf{R}_I - \mathbf{R}_J|} + \frac{1}{2}\sum_{i\neq j}\frac{e^2}{|\mathbf{r}_i - \mathbf{r}_j|} \\ &- \sum_{i,I}\frac{Z_I e^2}{|\mathbf{r}_i - \mathbf{R}_I|} \\ = &\, T_N + T_e + V_{NN} + V_{ee} + V_{eN}\end{aligned}$$

with capital indices referring to nuclei and lower-case indices referring to electrons, $\mathbf{R}_I$, Z_I and M_I are the position, atomic number mass of the I-th nucleus, m_e and $\mathbf{r}_i$ are the position and mass of the i-th electron. Terms of the first line on the right hand side are the total kinetic energy of the

nuclei (T_N) and the total kinetic energy of the electrons (T_e), respectively. Terms on the second line are the potential energies arising from Coulomb interactions between all the nuclei in the left term (V_{NN}) and all the electrons in the right term (V_{ee}). The term on the third line is the total interaction energy between the nuclei and the electrons (V_{eN}). The Schrödinger equation for this system is :

$$\mathcal{H}\Psi(\mathbf{r}_1, \mathbf{r}_2, ..., \mathbf{r}_N, \mathbf{R}_1, \mathbf{R}_2, ..., \mathbf{R}_N) = W\Psi(\mathbf{r}_1, \mathbf{r}_2, ..., \mathbf{r}_N, \mathbf{R}_1, \mathbf{R}_2, ..., \mathbf{R}_N),$$

where W and Ψ are the total energy and the wave function of the system.

In the Born-Oppenheimer approximation, the motion of electrons and nuclei are treated separately. Indeed, nuclei being much heavier than electrons, the time scale of their motion is much higher. The Hamiltonian of the system is then separable and we have an electronic and a nuclear part :

$$\mathcal{H} = H_N + H_e$$

where $H_N = T_N$ is the nuclear part and the electronic part is :

$$H_e(\mathbf{r}, \mathbf{R}) = -\frac{\hbar^2}{2m_e}\sum_i \boldsymbol{\nabla}_i^2 + V_{ext} + \frac{1}{2}\sum_{i\neq j}\frac{e^2}{|\mathbf{r}_i - \mathbf{r}_j|} = T_e + V_{ext} + V_{ee}.$$

The collective nuclear coordinates $\mathbf{R}$ are now treated as parameters for the electronic Hamiltonian and included in V_{ext}, and $\mathbf{r} = \{\mathbf{r}_i\}$ is a collective electron coordinate. The total wave function Ψ is a single product of the electronic wave function ϕ and and the nuclear wave function χ :

$$\Psi(\mathbf{r}, \mathbf{R}) = \phi(\mathbf{r})\chi(\mathbf{R})$$

This separated problem gives the following Schrödinger equations :

$$H_e(\mathbf{r}, \mathbf{R})\phi(\mathbf{r}, \mathbf{R}) = E_e(\mathbf{R})\phi(\mathbf{r}, \mathbf{R})$$

for the electronic part. E_e is the electronic energy eigenvalue, and we can obtain the potential energy surface $E_e(\mathbf{R})$ by solving this equation for different $\mathbf{R}$. For the nuclear problem, the Schrödinger equation writes :

$$\left[T_N + E_e(\mathbf{R})\right]\chi(\mathbf{R}) = E\chi(\mathbf{R}),$$

where the eigenvalue E is the total energy of the system.

1.2 Phonons

In this work we need to compute the normal modes of vibration of the crystals. In this chapter we will briefly introduce the theory of lattice vibrations, and the computation methods to calculate them.

Let start with the classical theory of phonons. Phonons are normal modes of vibration of the crystals. Since each mode has its own wavelength and momentum, we can treat the phonons as quasi-particles that have wavelength and momentum to each mode [21] [22].

1.2.1 Example of a linear chain

We consider a linear chain with a basis of two different atoms. The index α refers to the atom type in the unit cell, so that the masses of the atoms $\alpha = 1$ and $\alpha = 2$ are M_1 and M_2. Two atoms of the same type are separated by a distance a which is also the length of the N unit cells. We model the interaction between a pair of atoms inside the same unit cell by a spring with constant K and the pairs are coupled by a spring with constant G. We assume $K \leq G$.

We note $u_{n,\alpha}$ the displacement of the atom α in the unit cell n around its equilibrium position $r_{n,\alpha}$. We set ourselves in the harmonic approximation and assume only first-neighbor interactions. The potential energy for the ions writes :

$$\phi = \frac{K}{2}\sum_n (u_{n,1} - u_{n,2})^2 + \frac{G}{2}\sum_n (u_{n,2} - u_{n+1,1})^2.$$

Typically, lattice vibrations involve small movements of the atoms around their equilibrium positions, hence we can expand the potential like so :

$$\phi(r_{n,\alpha} + u_{n,\alpha}) = \phi(r_{n,\alpha}) + \frac{\partial \phi}{\partial r_{n,\alpha}} u_{n,\alpha} + \frac{1}{2}\frac{\partial^2 \phi}{\partial r_{n,\alpha}\partial r_{m,\beta}} u_{n,\alpha} u_{m,\beta},$$

where the index n refer to the n-unit cell and α to the atom in the basis. In our case, we have two atoms in the basis so we can have $\alpha = 1$ or $\alpha = 2$. The first two terms are zero : we take the

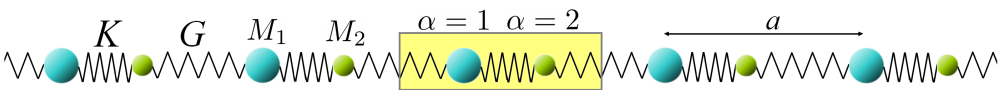

Figure 1.1: *Schematic description of the linear chain.*

potential to be zero at the equilibrium positions by convention, and the first derivative is evaluated at the equilibrium position so it vanishes. We define the matrix of interatomic force constants :

$$\Phi_{n\alpha}^{m\beta} = \frac{\partial^2 \phi}{\partial r_{n,\alpha} \partial r_{m,\beta}}.$$

We can now derive the force on each atom :

$$F_{n\alpha i} = -\frac{\partial \phi(r_{m\beta j} + u_{m\beta j})}{\partial u_{n\alpha i}}$$

where the i, j indices refer to the components of the cartesian coordinates. The equation of motion is :

$$-\Phi_{n\alpha i}^{m\beta j} u_{m\beta j} = M_\alpha \ddot{u}_{n\alpha i}.$$

We have three times the number of unit cells times the number of atoms per unit cells as a number of equations. We can decouple them thanks to Fourier transform and we have a solution of the form :

$$u_{n\alpha i} = \frac{1}{\sqrt{M_\alpha}} \epsilon_{\alpha i}(\mathbf{q}) e^{i(\mathbf{q}\cdot\mathbf{r}_n - \omega t)} \tag{1.1}$$

where $\epsilon_{\alpha i}(\mathbf{q})$ is the polarization vector for the oscillation. It is independent of n because of the translational invariance of the system. We impose Born-von Karman boundary conditions, *ie.* the last atom of the chain is bound to the first and this leads to :

$$e^{i(\mathbf{q}\cdot\mathbf{r}_N)} = e^{i(\mathbf{q}\cdot\mathbf{r}_0)} = 1$$

It implies that the norm of the vector $\mathbf{q}$ has the form :

$$q = \frac{2\pi}{a}\frac{n}{N}, \quad n \in \mathbb{N}$$

We can see that the displacement $u_{n\alpha}$ in equation 1.1 is unchanged by a translation of $\mathbf{q}$ by $2\pi/2$. Therefore there are only N values of $\mathbf{q}$ that yields consistent solutions. We take them between $-\pi/a$ and π/a. This interval is called the first Brillouin zone. The equation of motion becomes :

$$\omega^2 \epsilon_{\alpha i}(\mathbf{q}) = \frac{1}{\sqrt{M_\alpha M_\beta}} \Phi_{n\alpha i}^{m\beta j} e^{i(\mathbf{q}\cdot\mathbf{r}_n - \omega t)} \epsilon_{\beta j}(\mathbf{q})$$

where $m \neq n$ is the m-th unit cell, β is the index of the atom in this cell, $\beta = 1$ or $\beta = 2$, and the repeated indices are summed, as in Einstein notation. The translational invariance of the system gives :

$$\Phi_{n\alpha i}^{m\beta j} = \Phi_{0\alpha i}^{(m-n)\beta j}$$

so we can define the matrix element :

$$D_{\alpha i}^{\beta j} = \frac{1}{\sqrt{M_\alpha M_\beta}} \Phi_{n\alpha i}^{m\beta j} e^{i(\mathbf{q}\cdot\mathbf{r}_m - \mathbf{r}_n)} = \frac{1}{\sqrt{M_\alpha M_\beta}} \Phi_{0\alpha i}^{p\beta j} e^{i(\mathbf{q}\cdot\mathbf{r}_p)}$$

and the equation of motion becomes :

$$\omega^2 \epsilon_{\alpha i}(\mathbf{q}) = D_{\alpha i}^{\beta j} \epsilon_{\beta j}(\mathbf{q})$$

or

$$\left(D_{\alpha i}^{\beta j} - \omega^2 \delta_{\alpha i}^{\beta j} \right) \epsilon_{\beta j}(\mathbf{q}) = 0$$

We find the non-trivial solutions by solving the eigenvalue problem :

$$\det\big(\boldsymbol{D}(\mathbf{q}) - \omega^2 \mathbb{1}\big) = 0 \tag{1.2}$$

The dynamical matrix $\boldsymbol{D}$ must be Hermitian because the eigenvalues ω^2 real. We have :

$$\boldsymbol{D} = \begin{pmatrix} \dfrac{K+G}{M_1} & -\dfrac{K+Ge^{-iqa}}{\sqrt{M_1 M_2}} \\ -\dfrac{K+Ge^{iqa}}{\sqrt{M_1 M_2}} & \dfrac{K+G}{M_2} \end{pmatrix}$$

The secular equation 1.2 becomes :

$$\omega^4 - \omega^2 (K+G) \left(\frac{1}{M_1} + \frac{1}{M_2} \right) + \frac{4KG}{M_1 M_2} \sin^2(qa/2) = 0$$

and the solutions are :

$$\omega_\pm^2 = \frac{K+G}{2} \left(\frac{1}{M_1} + \frac{1}{M_2} \right) \pm \sqrt{\frac{(K+G)^2}{4} \left(\frac{1}{M_1} + \frac{1}{M_2} \right)^2 - \frac{4KG}{M_1 M_2} \sin^2(qa/2)}$$

The variation of ω with respect to $\mathbf{q}$ is called the dispersion relation. Let us determine the limits of this relation at the borders of the first Brillouin zone. In the limit $q \to 0$, the two solutions become :

$$\omega_+ = \sqrt{(K+G)\left(\frac{1}{M_1}+\frac{1}{M_2}\right)} \tag{1.3}$$

$$\omega_- = \sqrt{\frac{KG}{(K+G)(M_1+M_2)}}\ qa \tag{1.4}$$

and at the border $q = \pm\pi/a$:

$$\omega_+ = \sqrt{\frac{2K}{M_1}} \tag{1.5}$$

$$\omega_- = \sqrt{\frac{2G}{M_2}} \tag{1.6}$$

We only take positive values for the solutions, since they are physical frequencies. We plot the dispersion relation in figure 1.2.

Consider the branch corresponding to the solution ω_- at $q = 0$. When substituting the solution 1.3 into the motion equation 1.2.1, we obtain the amplitude ratio :

$$\frac{\epsilon_2}{\epsilon_1} = -\sqrt{\frac{M_1}{M_2}},$$

It means that the modes of vibration in this branch have their ions moving out of phase with one another in each unit cell. If the ions had an opposite charge, it would create an oscillating electric dipole, able to interact with external electromagnetic waves, like an optical field. This branch is called the *optical branch*.

Similarly, for the branch corresponding to the solution ω_-, for the case $q = 0$, the solution vanishes hence the amplitude ratio is :

$$\frac{\epsilon_2}{\epsilon_1} = +\sqrt{\frac{M_2}{M_1}}$$

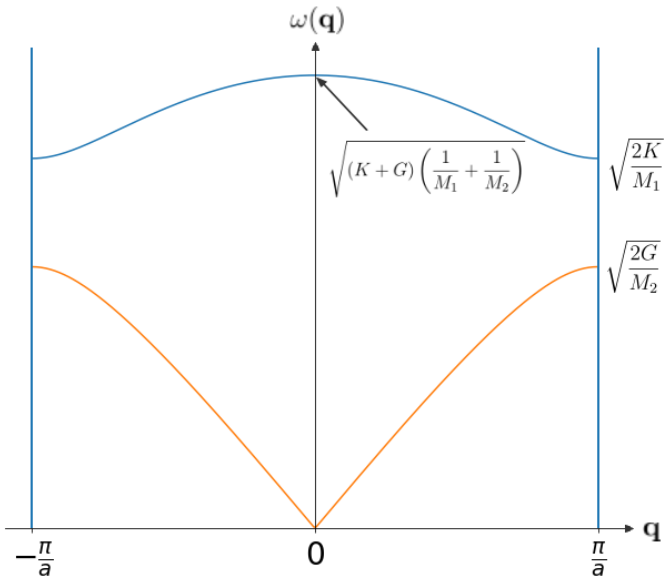

Figure 1.2: *Dispersion relation for the diatomic linear chain. The blue curve is the optical branch corresponding to the solution ω_+ and the orange curve is the acoustic branch corresponding to the solution ω_-.*

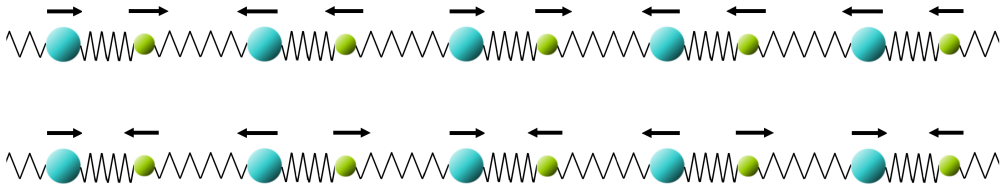

Figure 1.3: *Sketch of examples of a vibration mode of the acoustic branch (top) where the ions in the same unit cell move in phase, and a vibration mode of the optical branch (bottom) where the ions in the same unit cell move out of phase.*

It means that the ions in each unit cell are moving in phase with one another. As it is linear for small $\mathbf{q}$, it resembles an acoustic wave with long wavelength, hence it is called an *acoustic branch*.

Notice that for $q = \pm\pi/a$, the two branches are flat. It means that the derivative $d\omega/d\mathbf{q}$ is zero.

This derivative is also known as the group velocity of a wave packet. This shows that the wave is stationary at the border of the first Brillouin zone.
Note that in the case where $K = G$ and $M_1 = M_2$, the two branches would be degenerate in $q = \pm\pi/a$. It would correspond to a linear chain of identical atoms, with the particularity of having two atoms per unit cell, which gives two branches.

1.2.2 Symmetries and invariances of the dynamical matrix

In general, for any three-dimensional crystal with p atoms per unit cell and N unit cells, the number of degrees of freedom is $3pN$. One can show that there are N values of $\mathbf{q}$ for each branch. The total number of branches or modes is then $3p$, 3 of them being acoustic branches and $3p-3$ optical branches.We can make use of symmetries and invariances of the lattice to get more information about the dispersion.

First, let us show that $\omega_\pm^2$ is real. The complex conjugate of the dynamical matrix elements are :

$$\begin{aligned} D_{\alpha i}^{*\beta j} &= \frac{1}{\sqrt{M_\alpha M_\beta}} \Phi_{0\alpha i}^{p\beta j} e^{-i(\mathbf{q}\cdot\mathbf{r}_p)} \\ &= \frac{1}{\sqrt{M_\alpha M_\beta}} \Phi_{0,\alpha,i}^{-p,\beta,j} e^{i(\mathbf{q}\cdot\mathbf{r}_p)} \end{aligned}$$

Then thanks to the symmetry of the second derivative :

$$D_{\alpha i}^{*\beta j} = \frac{1}{\sqrt{M_\alpha M_\beta}} \Phi_{-p,\beta,j}^{0,\alpha,i} e^{i(\mathbf{q}\cdot\mathbf{r}_p)} = \frac{1}{\sqrt{M_\alpha M_\beta}} \Phi_{0,\beta,j}^{p,\alpha,i} e^{i(\mathbf{q}\cdot\mathbf{r}_p)} = D_{\beta j}^{\alpha i}$$

Thus, $\mathbf{D}^{\top *} = \mathbf{D}^\dagger = \mathbf{D}$ so $\mathbf{D}$ is hermitian and its eigenvalues $\omega_\pm^2$ are real. Then $\omega_\pm$ can either be real or pure imaginary. In the latter case, the Fourier transform of the solution would grow exponentially, which means that the system considered is unstable.

Second, let us consider the time-reversal invariance. We have solutions for the displacements in the form of plane waves:

$$u_{n\alpha i} = \frac{1}{\sqrt{M_\alpha}} \epsilon_{\alpha i}(\mathbf{q}) e^{i(\mathbf{q}\cdot\mathbf{r}_n - \omega t)}$$

We assume the wave is propagating in the direction of positive x such that $\mathbf{q} = \hat{x} q_x$. Then the coordinate of the plane of stationary phase is :

$$x = \frac{\omega}{q_x} t.$$

Now it is clear that changing the sign of th direction of propagation of the wave q_x is equivalent to taking $t \to -t$. Under time-reversal, the frequencies are conserved so we have :

$$\omega(-\mathbf{q}) = \omega(\mathbf{q}).$$

This is equivalent to $D^{\alpha i}_{\beta j}(\mathbf{q}) = D^{*\alpha i}_{\beta j}(-\mathbf{q})$, from the definition of $\mathbf{D}$. Now we go back to the secular equation :

$$\left(D^{\beta j}_{\alpha i}(\mathbf{q}) - \omega^2(\mathbf{q}) \delta^{\beta j}_{\alpha i} \right) \epsilon_{\beta j}(\mathbf{q}) = 0$$

The ϵ are the normalized eigenvectors of $\mathbf{D}$, *ie.* they are the elements of a unitary matrix that diagonalizes $\mathbf{D}$. They foolow orthogonality and completeness relations :

$$\sum_{\alpha,i} \epsilon^{*(n)}_{\alpha,i}(\mathbf{q}) \epsilon^{(m)}_{\alpha,i}(\mathbf{q}) = \delta_{m,n}$$
$$\sum_{n} \epsilon^{*(n)}_{\alpha,i}(\mathbf{q}) \epsilon^{*(n)}_{\beta,j}(\mathbf{q}) = \delta_{\alpha,\beta} \delta_{i,j}$$

Now we take the complex conjugate of the secular equation :

$$\left(D^{\beta j}_{\alpha i}(-\mathbf{q}) - \omega^2(-\mathbf{q}) \delta^{\beta j}_{\alpha i} \right) \epsilon^{*}_{\beta j}(\mathbf{q}) = 0$$

The we must have :

$$\epsilon^{*}_{\beta j}(\mathbf{q}) \propto \epsilon_{\beta j}(-\mathbf{q}).$$

Since the ϵ are normalized, the constant of proportionality may be chosen to be one and :

$$\epsilon^{*}_{\beta j}(\mathbf{q}) = \epsilon_{\beta j}(-\mathbf{q})$$

Third, the point group symmetry of the real and reciprocal lattice must be found in the dispersion relations. For example, the dispersion relation has the same periodicity than the Brillouin zone. Taking a vector of the reciprocal lattice $\mathbf{G}$, we have $D^{\beta j}_{\alpha i}(\mathbf{q}+\mathbf{G}) = D^{\beta j}_{\alpha i}(\mathbf{q})$ since $\mathbf{G} \cdot \mathbf{r}_p = 2\pi n$ with $n \in \mathbb{N}$. $\mathbf{D}$ is periodic in $\mathbf{q}$-space, so must be its eigenvalues and eigenvectors :

$$\omega^{(n)}(\mathbf{q}+\mathbf{G}) = \omega^{(n)}(\mathbf{q})$$
$$\epsilon_{\beta j}(\mathbf{q}+\mathbf{G}) = \epsilon_{\beta j}(\mathbf{q})$$

Finally, let us consider the translational invariance of the interatomic forces constants matrix $\mathbf{\Phi}$. If we shift the atoms in all sites n and all elements of the basis α by the same arbitrary dislacement $s_{n,\alpha,i} = s_{1,1,i}$, the energy of the system is unchanged because the interaction depends only on the distance between ions, not on their arbitrary position in space :

$$\begin{aligned}\delta E &= \frac{1}{2}\sum_{m,n,\alpha,\beta,i,j} \Phi_{0,\alpha,i}^{m-n,\beta,j} s_{n,\alpha,i} s_{m,\beta,j} = 0 \\ &= \frac{1}{2}\sum_{i,j} s_{1,1,i} s_{1,1,j} \sum_{m,n,\alpha,\beta} \Phi_{0,\alpha,i}^{m-n,\beta,j}\end{aligned}$$

Since the displacement $s_{1,1,i}$ is finite, it must be :

$$\sum_{m,n,\alpha,\beta} \Phi_{0,\alpha,i}^{m-n,\beta,j} = \sum_{p,\alpha,\beta} \Phi_{0,\alpha,i}^{p,\beta,j} = 0$$

This translates to the fact that the translation of the whole lattice corresponds to a $\mathbf{q} = 0$, and since no energy is gained by the lattice, it must be that $\omega_\nu(\mathbf{q} = 0) = 0$ for the branch ν which contains this mode. It resembles an acoustic mode, since it is linear in $\mathbf{q}$. The acoustic mode can be obtained by perturbation in $\mathbf{q}$ around this translational mode.

1.2.3 Normal modes and quantization

Let us now derive the phonon modes in a quantum approach. We can define the canonical momenta and coordinates P_μ and Q_ν that obey the relation :

$$P_\nu^*(\mathbf{q}) = \frac{\partial L}{\partial Q_\nu(\mathbf{q})} = \dot{Q}_\mu^*(\mathbf{q})$$

where the indices μ and ν denote modes and L is the Lagrangian of the system :

$$L = T - V = \frac{1}{2}\sum_{\mathbf{q},\mu}\left(\left|\dot{Q}_\mu(\mathbf{q})\right|^2 - \omega^2 \left|Q_s(\mathbf{q})\right|^2\right)$$

The Euler-Lagrange equations of motion are :

$$\frac{d}{dt}\left(\frac{\partial L}{\partial \dot{Q}^*_\mu}(\mathbf{k})\right) - \frac{\partial L}{\partial Q^*_\mu} = 0 \quad \text{or} \quad \ddot{Q}_\mu(\mathbf{q}) + \omega^2_\mu(\mathbf{q}) Q_\mu(\mathbf{q}) = 0$$

for each $\mathbf{q}, \mu$. These are equations for $3pN$ (p the number of atoms in a unit cell, N the number of unit cells) independent harmonic osillators.

Now we can perform the second quantization by setting the relation :

$$[Q^*_\nu(\mathbf{q}), P_\mu(\mathbf{k})] = i\hbar\delta_{\mathbf{q},\mathbf{k}}\delta_{\nu,\mu}$$

and introducing the annihilation and creation quantum operators :

$$a_\mu(\mathbf{q}) = \frac{1}{\sqrt{2\hbar}}\left(\sqrt{\omega_\mu(\mathbf{q})}Q_\mu(\mathbf{q}) + \frac{i}{\sqrt{\omega_\mu(\mathbf{q})}}P_\mu(\mathbf{q})\right)$$
$$a^\dagger_\mu(\mathbf{q}) = \frac{1}{\sqrt{2\hbar}}\left(\sqrt{\omega_\mu(\mathbf{q})}Q^*_\mu(\mathbf{q}) - \frac{i}{\sqrt{\omega_\mu(\mathbf{q})}}P^*_\mu(\mathbf{q})\right)$$

or also

$$Q_\mu(\mathbf{q}) = \sqrt{\frac{\hbar}{2\omega_\mu(\mathbf{q})}}\left(a_\mu(\mathbf{q}) + a^\dagger_\mu(-\mathbf{q})\right)$$
$$P_\mu(\mathbf{q}) = -i\sqrt{\frac{\hbar\omega_\mu(\mathbf{q})}{2}}\left(a_\mu(\mathbf{q}) - a^\dagger_\mu(-\mathbf{q})\right)$$

where

$$\left[a_\mu(\mathbf{q}), a^\dagger_\nu(\mathbf{k})\right] = \delta_{\nu,\mu}\delta_{\mathbf{k},\mathbf{q}} \quad [a_\mu(\mathbf{q}), a_\nu(\mathbf{k})] = \left[a^\dagger_\mu(\mathbf{q}), a^\dagger_\nu(\mathbf{k})\right] = 0$$

This transformation $\{Q, P\} \to \left\{a, a^\dagger\right\}$ is canonical since it preserves the commutator algebra from equation 1.2.3 and the Hamiltonian becomes :

$$H = \sum_{\mathbf{q},\mu}\hbar\omega_\mu(\mathbf{q})\left(a^\dagger_\mu(\mathbf{q})a_\mu(\mathbf{q}) + \frac{1}{2}\right)$$

which is a sum over $3pN$ independent quantum oscillators. Each of this mode is referred to as a phonon mode.

1.3 Density Functional Theory

In despise of the great simplification of the problem thanks to the Born-Oppenheimer approximation, the electronic equation cannot be solved analytically because of the Coulombian interaction between electrons V_{ee} which is singular close the nuclei. Therefore we need to use other approximations to be able to solve these problems. Density Functional Theory (DFT) was introduced by Hohenberg and Kohn in 1964 [23] and Kohn and Sham in 1965 [24]. It allows to treat a many-body problem using the groundstate electronic density instead of the wavefunction.

1.3.1 Hohenberg-Kohn theorems

DFT is based on two theorems relating to any system with N interacting electrons in an external potential $V_{ext}(\mathbf{r})$. The first theorem states :

Theorem 1 *The total energy of the system is a unique functional of the electronic density $n(\boldsymbol{r})$.*

Let us prove it by contradiction. Assume there exist two external potentials $V^1_{ext}(\mathbf{r})$ and $V^2_{ext}(\mathbf{r})$ that differ by more than a constant that induce the same electronic density $n(\mathbf{r})$. The two potentials are part of two different Hamiltonians $H^{(1)}$ and $H^{(2)}$ with different eigen-wavefunctions $\left|\Psi^{(1)}\right\rangle$ and $\left|\Psi^{(2)}\right\rangle$. These wavefunctions are describing the fundamental state of each Hamiltonian. Then we have :

$$E^{(1)} = \left\langle \Psi^{(1)} \right| H^{(1)} \left| \Psi^{(1)} \right\rangle < \left\langle \Psi^{(2)} \right| H^{(1)} \left| \Psi^{(2)} \right\rangle . \tag{1.7}$$

This inequality holds if the fundamental state is non degenerate. We can write the term on the right hand side as :

$$\begin{aligned} \left\langle \Psi^{(2)} \right| H^{(1)} \left| \Psi^{(2)} \right\rangle &= \left\langle \Psi^{(2)} \right| H^{(2)} \left| \Psi^{(2)} \right\rangle + \left\langle \Psi^{(2)} \right| H^{(1)} - H^{(2)} \left| \Psi^{(2)} \right\rangle \\ &= E^{(2)} + \int \left[V^1_{ext}(\mathbf{r}) - V^2_{ext}(\mathbf{r}) \right] n(\mathbf{r}) d^3\mathbf{r} \end{aligned}$$

which leads to :

$$E^{(1)} < E^{(2)} + \int \left[V^1_{ext}(\mathbf{r}) - V^2_{ext}(\mathbf{r}) \right] n(\mathbf{r}) d^3\mathbf{r}. \tag{1.8}$$

The inequality in equation 1.7 still holds if we exchange the superscripts 1 and 2. Thus we have a similar expression for $E^{(2)}$:

$$E^{(2)} < E^{(1)} + \int \left[V^2_{ext}(\mathbf{r}) - V^1_{ext}(\mathbf{r})\right] n(\mathbf{r}) d^3\mathbf{r}. \tag{1.9}$$

And now if we sum equations 1.8 and 1.9, we obtain a contradictory inequality :

$$E^{(1)} + E^{(2)} < E^{(1)} + E^{(2)}.$$

It means that the initial assumption cannot be true. Therefore there cannot exist two different external potentials that differ by more than a constant and that give the same electronic density for a non degenerate ground state. This proves the first Hohenberg and Kohn theorem. This theorem allows a different approach to solve the many-electron problem : the goal of DFT is to express the energy of the system as a functional of the density rather than trying to approximate the wavefunction. A consequence of this theorem is that the density uniquely determines the Hamiltonian, as well as any observable, hence the energy of the system is a unique functional of $n(\mathbf{r})$. It writes :

$$E[n(\mathbf{r})] = \int n(\mathbf{r}) V_{ext}(\mathbf{r}) d^3\mathbf{r} + F_{HK}[n(\mathbf{r})] \tag{1.10}$$

where $F_{HK}[n(\mathbf{r})]$ is the part of the functional that does not depend on the external potential and is called the Hohenberg-Kohn universal functional :

$$F_{HK}[n(\mathbf{r})] = \langle \Psi(\mathbf{r}) | \, T_e + V_{ee} \, | \Psi(\mathbf{r}) \rangle$$

It is valid for any number of particles and any external potential. The energy functional in equation 1.10 is the ground state energy for the correct density $n(\mathbf{r})$. The aim of the second theorem is to find the correct $n(\mathbf{r})$

The second theorem is a variational principle that states :

Theorem 2 *For a given number of particles and external potential, the ground state energy of the system is the value that minimizes the universal energy functional $E[n(\boldsymbol{r})]$, and the associated density corresponds to the exact ground state density.*

This holds assuming that the set of densities with respect to which the energy functional is minimized are constrained to conserve the total number of particles :

$$\int n(\mathbf{r}) d^3\mathbf{r} = N$$

and

$$n(\mathbf{r} \to \infty) = 0$$

As stated before, any observable is a functional of the density, thus we can write the expectation value of F_{HK} as :

$$F_{HK}[n(\mathbf{r})] = \langle \Psi | \, F_{HK} \, | \Psi \rangle \, .$$

Let us consider another density $n'(\mathbf{r})$, associated with a state $|\Psi'\rangle$, that arise from the potential V_{ext}. Since the energy functional is universal, one can write :

$$E_{V_{ext}}[n'(\mathbf{r})] = \int n'(\mathbf{r}) V_{ext}(\mathbf{r}) d^3\mathbf{r} + F_{HK}[n'(\mathbf{r})],$$

and according to the variational principle :

$$\langle \Psi' | \, F_{HK} \, | \Psi' \rangle + \langle \Psi' | \, V_{ext} \, | \Psi' \rangle > \langle \Psi | \, F_{HK} \, | \Psi \rangle + \langle \Psi | \, V_{ext} \, | \Psi \rangle$$

where Ψ is the wavefunction associated with the correct ground state density $n(\mathbf{r})$. This leads to :

$$\int n'(\mathbf{r}) V_{ext}(\mathbf{r}) d^3\mathbf{r} + F_{HK}[n'(\mathbf{r})] > \int n(\mathbf{r}) V_{ext}(\mathbf{r}) d^3\mathbf{r} + F_{HK}[n(\mathbf{r})]$$

and the second theorem is proved, since :

$$E_{V_{ext}}[n'(\mathbf{r})] > E_{V_{ext}}[n(\mathbf{r})],$$

that is, the correct ground state density yields a lower energy functional than any other density. According to these two theorems, solving the Schrödinger equation amounts to minimize the energy functional $E[n(\mathbf{r})] = \langle \Psi | \, T_e + V_{ee} + V_{ext} \, | \Psi \rangle$. As we saw, the knowledge of the Hohenberg-Kohn functional $F_{HK}[n(\mathbf{r})]$ would be enough to determine the total energy of the system and its ground state properties. However the exact form of this functional is still unknown to this day. It is needed to use extra approximations to make use of the Hohenberg and Kohn theorems.

1.3.2 Kohn-Sham equations

In their paper from 1965 [24], Kohn and Sham proposed a formulation that maps the full interacting system with the real potential, onto a fictitious non-interacting system in which the electrons are in a single-particle potential v_{KS}. Both systems are assumed to have the same electronic density $n(\mathbf{r})$ by construction. The idea is to switch the interacting electron problem to an independent electron problem, since the kinetic energy of a gas of interacting electrons is unknown.
The Hamiltonian of the non-interacting system is separable since the electrons are independent :

$$H = \sum_i h_i = \sum_i \left[-\frac{\hbar^2}{2m}\boldsymbol{\nabla}^2 + v_{KS}(\mathbf{r}) \right]$$

Then Schrödinger equation a system of uncoupled equations for each occupied state $\phi_i(\mathbf{r})$:

$$\left[-\frac{\hbar^2}{2m}\boldsymbol{\nabla}^2 + v_{KS}(\mathbf{r}) \right] \phi_i(\mathbf{r}) = \epsilon_i \phi_i(\mathbf{r}).$$

Now let us derive the Kohn-Sham potential v_{KS}. The total energy functional of the non-interacting system is :

$$E_{NI}[n(\mathbf{r})] = T_{NI}[n(\mathbf{r})] + V_{KS}[n(\mathbf{r})],$$

where

$$V_{KS}[n(\mathbf{r})] = \int v_{KS}(\mathbf{r}) n(\mathbf{r}) d^3\mathbf{r}.$$

On the other hand, the total energy functional of the real interacting system is :

$$E_I[n(\mathbf{r})] = T_{NI}[n(\mathbf{r})] + E_H[n(\mathbf{r})] + E_{XC}[n(\mathbf{r})] + V_{ext}[n(\mathbf{r})],$$

where E_H is the Hartree energy :

$$E_H[n(\mathbf{r})] = \frac{1}{2} \int e^2 \frac{n(\mathbf{r}) n(\mathbf{r}')}{|\mathbf{r} - \mathbf{r}'|} d^3\mathbf{r} d^3\mathbf{r}'$$

and E_{XC} is the exchange-correlation energy, that contains the following terms :

$$E_{XC} = T_I[n] - T_{NI} - E_H[n] + V_{ee} = F_{HK} - T_{NI}[n] - E_H[n].$$

Applying the variational principle to $E_{NI}[n]$ and $E_I[n]$, we obtain :

$$\frac{\delta E_{NI}[n]}{\delta n}\Big|_{n_0} = 0 \implies \frac{\delta T_{NI}[n]}{\delta n}\Big|_{n_0} = -v_{KS}(\mathbf{r})$$
$$\frac{\delta E_{I}[n]}{\delta n}\Big|_{n_0} = 0 \implies \frac{\delta T_{NI}[n]}{\delta n}\Big|_{n_0} = -v_{H}(\mathbf{r}) - \frac{\delta E_{XC}[n]}{\delta n}\Big|_{n_0} - v_{ext}(\mathbf{r})$$

where n_0 is the ground state density. Combining the two equations, we obtain the expression of the Kohn-Sham potential :

$$v_{KS}(\mathbf{r}) = v_{ext}(\mathbf{r}) + v_H(\mathbf{r}) + v_{XC}(\mathbf{r})$$

with the Hartree potential :

$$v_H(\mathbf{r}) = \frac{\delta E_H[n(\mathbf{r})]}{\delta n(\mathbf{r})}\Big|_{n_0} = e^2 \int \frac{n(\mathbf{r}')}{|\mathbf{r} - \mathbf{r}'|} d^3\mathbf{r}'$$

and the exchange-correlation potential :

$$v_{XC}(\mathbf{r}) = \frac{\delta E_{XC}[n(\mathbf{r})]}{\delta n(\mathbf{r})}\Big|_{n_0}$$

Now we can write the Kohn-Sham equations :

$$\left[-\frac{\hbar^2}{2m}\boldsymbol{\nabla}^2 - e^2 \sum_I \frac{Z_I}{|\mathbf{R}_I - \mathbf{r}|} + e^2 \int \frac{n(\mathbf{r}')}{|\mathbf{r} - \mathbf{r}'|} d^3\mathbf{r}' + v_{XC}(\mathbf{r}) \right] \varphi_i(\mathbf{r}) = \varepsilon_i \varphi_i(\mathbf{r})$$

This is different from the Schrödinger equation for the ε_i are not the eigenvalues of the energy but Lagrange multipliers related to the orthonormality of the single-particle states $\varphi_i(\mathbf{r})$. Solving the equations for each state gives access to the electronic density of the non-interacting system $n_{NI}(\mathbf{r})$ which is equal to the density of the real interacting system $n_I(\mathbf{r})$ by construction :

$$n_{NI}(\mathbf{r}) = n_I(\mathbf{r}) = \sum_i |\varphi_i(\mathbf{r})|^2$$

However since the Hartree and the exchange-correlation potentials depend on the density, Kohn-Sham equations must be solved self-consistently. Once solved, we can multiply the equations by the complex conjugate of the wave functions, integrate over space and sum all the single-particle states to obtain :

$$T_{NI}[n(\mathbf{r})] = \sum_i \varepsilon_i - \int n(\mathbf{r}) v_{ext}(\mathbf{r}) d^3\mathbf{r} - \int n(\mathbf{r}) v_H(\mathbf{r}) d^3\mathbf{r} - \int n(\mathbf{r}) v_{XC}(\mathbf{r}) d^3\mathbf{r}$$

which is the kinetic energy of the non-interacting system. Now we can derive the expression for the total energy of the interacting system.

$$E_I[n(\mathbf{r})] = \sum_i \varepsilon_i - \frac{1}{2}\int\int \frac{n(\mathbf{r})n(\mathbf{r}')}{|\mathbf{r}-\mathbf{r}'|}d^3\mathbf{r}d^3\mathbf{r}' + E_{XC}[n(\mathbf{r})] - \int n(\mathbf{r})v_{XC}(\mathbf{r})d^3\mathbf{r}$$

Up to this point, the Density Functional Theory is an exact theory. However in general the exchange-correlation functional is unknown. Therefore one needs approximations to compute it.

1.3.3 Exchange-correlation approximation

In order to approximate the exact exchange-correlation functional, we introduce the quantity $n_{XC}(\mathbf{r},\mathbf{r}')$ which is the exchange-correlation hole. It is a zone around each electron of an interacting system where the probability of finding another electron is reduced. It arises from the fact that two electrons repel one another.

Another key idea is to tune the electronic interactions with a coupling constant λ. With a fixed electronic density, $\lambda = 1$ represents the fully interacting, physical system, while $\lambda = 0$ represents the non-interacting, fictitious system. Then we can express the exchange-correlation functional in terms of an integral over the coupling constant λ :

$$E_{XC}[n(\mathbf{r})] = \frac{1}{2}\int n(\mathbf{r})d^3\mathbf{r}\int \frac{n_{XC}(\mathbf{r},\mathbf{r}')}{|\mathbf{r}-\mathbf{r}'|}d^3\mathbf{r}'$$

where the exchange-correlation hole $n_{XC}(\mathbf{r},\mathbf{r}')$ is averaged over a coupling-constant dependent hole $n^{\lambda}_{XC}(\mathbf{r},\mathbf{r}')$ given by :

$$n_{XC}(\mathbf{r},\mathbf{r}') = \int_0^1 n^{\lambda}_{XC}(\mathbf{r},\mathbf{r}')d\lambda.$$

The exchange-correlation functional can be seen as the energy resulting from the interaction between an electron and its exchange-correlation hole. The latter follows a sum rule :

$$\int n_{XC}(\mathbf{r},\mathbf{r}')d^3\mathbf{r}' = -1.$$

This implies that the exchange-correlation hole has a deficit of exactly one electron, therefore an electron and its hole have no net charge.

Now we can define another useful quantity, the exchange-correlation energy per particle :

$$\varepsilon_{XC}[n(\mathbf{r})] = \frac{1}{2}\int \frac{n_{XC}(\mathbf{r},\mathbf{r}')}{|\mathbf{r}-\mathbf{r}'|}d^3\mathbf{r}'$$

Once this quantity is defined, we can write the exchange-correlation energy functional as :

$$E_{XC}[n(\mathbf{r})] = \int n(\mathbf{r})\varepsilon_{XC}[n(\mathbf{r})]d^3\mathbf{r}.$$

This is the quantity we want to approximate in order to obtain a solution. The different types of approximation differ on the way they construct the exchange-correlation energy per particle by sampling the density around each electron.

In fact it is exact

1.3.4 Local Density Approximation

The first and oldest approximation for the energy functional is the local density approximation (LDA). It was proposed by Hohenberg and Kohn in their original DFT paper [23]. It consists of locally replacing the true exchange-correlation energy of a system with the exchange-correlation energy of an homogeneous electron gas with the same density. Indeed, the homogeneous electron gas is the only system for which the exchange-correlation energy is known exactly. In the LDA, the total energy functional is written as :

$$E_{XC}^{LDA}[n(\mathbf{r})] = \int n(\mathbf{r})\varepsilon_{XC}^{hom}[n(\mathbf{r})]d^3\mathbf{r}.$$

It can be separated into an exchange and a correlation term :

$$E_{XC}^{LDA}[n(\mathbf{r})] = E_{X}^{LDA}[n(\mathbf{r})] + E_{C}^{LDA}[n(\mathbf{r})] = \int n(\mathbf{r})\varepsilon_{X}^{hom}[n(\mathbf{r})]d^3\mathbf{r} + \int n(\mathbf{r})\varepsilon_{C}^{hom}[n(\mathbf{r})]d^3\mathbf{r}.$$

The exchange term can be computed using the functional form of the exchange energy for the homogeneous electron gas [25] :

$$E_{X}^{LDA}[n(\mathbf{r})] = -\frac{3}{4}\left(\frac{3}{\pi}\right)^{1/3}\int n(\mathbf{r})^{4/3}d\mathbf{r}.$$

The correlation term is determined from an interpolation formula, with coefficients fixed for example from the data generated by Ceperley and Alder using quantum Monte Carlo simulations of jellium [26].

The LDA has been very successful and gives good results for system with slowly varying electronic density, such as solids. However, the LDA usually underestimates the band gap.

1.3.5 Generalized Gradient Approximation

Perdew proposed a way to go beyond the LDA in 1985 [27]. It is called the generalized gradient approximation (GGA) and is based on an series expansion in terms of density gradient. The full series expansion was called the gradient expansion approximation, but it violated important physical conditions on the exchange hole. Perdew and others proposed a cutoff procedure on the real-space exchange correlation hole that respects the physical conditions previously violated. Hence we can write the GGA in terms of an analytic function $F_{XC}[n(\mathbf{r}), \boldsymbol{\nabla} n(\mathbf{r})]$, called the enhancement factor, that depends on both the density and its gradient and that modifies the exchange-correlation energy of the LDA :

$$E_{XC}^{GGA}[n(\mathbf{r})] = \int n(\mathbf{r}) \varepsilon_{XC}^{hom}[n(\mathbf{r})] F_{XC}[n(\mathbf{r}), \boldsymbol{\nabla} n(\mathbf{r})] d^3\mathbf{r}$$

The GGA allows more accurate results than the LDA, especially for molecules. There exist different form of the enhancement factor that give birth to different GGA functionals. One of the most used was proposed by Perdew, Burke and Ernzerhof in 1996 [28].

There are other types of approximation for the exchange-correlation energy functional. The meta-GGA includes higher derivatives of the density to the approximation, as well as the kinetic energy. The so-called hybrid functionals are combining the exact Hartree-Fock exchange functional with exchange and correlation GGA functionals. Finally, non-local functionals model the exchange-correlation hole with analytic functions and are fully non-local. Each of these types of approximation have their advantages and shortcomings and are used in diverse fields.

1.3.6 Kohn-Sham formulation in plane waves

We now present the implementation of the Kohn-Sham formulation of DFT in plane waves, as it is well adapted for the study of infinite periodic systems like crystals. It is the formulation coded in the software we used for this work to perform all the DFT calculations, QUANTUM ESPRESSO [29, 30, 31].

Let us start off by saying that the square of the wavefunction $|\psi_{j,\mathbf{k}}|^2$ of an electron into a periodic

crystalline potential has the same periodicity than the potential. This is Bloch's theorem [32] and it writes mathematically :

$$\psi_{j,\mathbf{k}}(\mathbf{r}) = u_j(\mathbf{r})e^{i\mathbf{k}\cdot\mathbf{r}}, \tag{1.11}$$

where j denotes the band index and $\mathbf{k}$ the wave vector, confined to the first Brillouin zone of the reciprocal lattice. $u_j(\mathbf{r})$ has the same periodicity than the lattice and can be expressed in plane waves, with wavevectors $\mathbf{G}$ that are the vectors of the reciprocal lattice :

$$u_j(\mathbf{r}) = \sum_{\mathbf{G}} c_{j,\mathbf{G}} e^{i\mathbf{G}\cdot\mathbf{r}} \tag{1.12}$$

where $c_{j,\mathbf{G}}$ are the plane waves coefficients. Consequently we can write the wavefunction of the electron in band j as :

$$\psi_{j,\mathbf{k}}(\mathbf{r}) = \sum_{\mathbf{G}} c_{j,\mathbf{k}+\mathbf{G}} e^{i(\mathbf{k}+\mathbf{G})\cdot\mathbf{r}}.$$

Now if we write the total local potential as a sum of all the contributions :

$$V(\mathbf{r}) = \sum_{\mathbf{G}} \overline{V}(\mathbf{G}) e^{i\mathbf{G}\cdot\mathbf{r}},$$

where $\overline{V}(\mathbf{G})$ is the Fourier transform of the potential in real space, we obtain a simpler expression of the Kohn-Sham equations in reciprocal-space :

$$\sum_{\mathbf{G}'} \Big[\frac{1}{2} |\mathbf{k}+\mathbf{G}|^2 \delta_{\mathbf{G},\mathbf{G}'} + \overline{V}_{ext}(\mathbf{G}-\mathbf{G}') + \overline{V}_H(\mathbf{G}-\mathbf{G}') + \overline{V}_{XC}(\mathbf{G}-\mathbf{G}') \Big] c_{j,\mathbf{k}+\mathbf{G}'} = \varepsilon_i(\mathbf{k}) c_{j,\mathbf{k}+\mathbf{G}}.$$

The first term is the kinetic contribution and is diagonal. For the calculation to be exact we would need an infinite sum over the $\mathbf{G}$ vectors. However we can truncate the sum since the first terms have the higher contribution. We truncate the sum at E_{cut} such that :

$$\frac{1}{2} |\mathbf{k}+\mathbf{G}|^2 \leq E_{cut}.$$

One needs to check for the convergence of the results with respect to E_{cut}. The advantage is that the precision of the results can be improved by increasing E_{cut}. However, the number of plane waves

required to describe highly curved wavefunctions lengthen the calculations. This is especially the case in the core region of atoms. We will present a way to workaround it below.

1.3.7 Brillouin zone sampling

A consequence of Bloch's theorem in equations 1.11 and 1.12 is that since the wavefunctions are periodic, the set of unique wavevectors $\{\mathbf{k}\}$ is contained in an interval called the first Brillouin zone, outside of which a wavevector $\mathbf{k}'$ can be translated back into it. Effectively we can replace any integral over a periodic system in real space by an integral in reciprocal space over the first Brillouin zone, by integrating over infinitely many points in reciprocal space. We name these points **k**-points. In practice, we can integrate over a dense, finite mesh of **k**-points, because the electron wavefunctions do not vary too much over small distances in reciprocal space. We can replace the integral of any function $f(\mathbf{r})$ by a weighted discrete sum :

$$\int_{BZ} F(\mathbf{k}) d\mathbf{k} = \frac{1}{\Omega} \sum_j w_j F(\mathbf{k}_j)$$

where $F(\mathbf{k})$ is the Fourier transform of $f(\mathbf{r})$, Ω is the volume of the crystal primitive cell and w_j are the weights. The number of **k**-points has an influence on the precision of the results, therefore it must be tuned by checking the convergence of the total energy when increasing the number of **k**-points. One approach to pick the positions of the **k**-points is the Monkhorst-Pack method [33], in which the **k**-points are homogeneously distributed in reciprocal space in a grid that has the same shape than the Brillouin zone :

$$\mathbf{k}_j = x_{1j}\mathbf{b}_j + x_{2j}\mathbf{b}_2 + x_{3j}\mathbf{b}_3$$

where $\mathbf{b}_1, \mathbf{b}_2, \mathbf{b}_3$ are the reciprocal lattice vectors and

$$x_{ij} = \frac{l_i}{n_j}, \quad j = 1, ..., n_j$$

where l_i are the lengths of the reciprocal lattice vectors and n_j is the number of special **k**-points in the set. Generally, the symmetries of the crystal are used to reduce even more the number of **k**-points needed, by according the corresponding weights w_j.

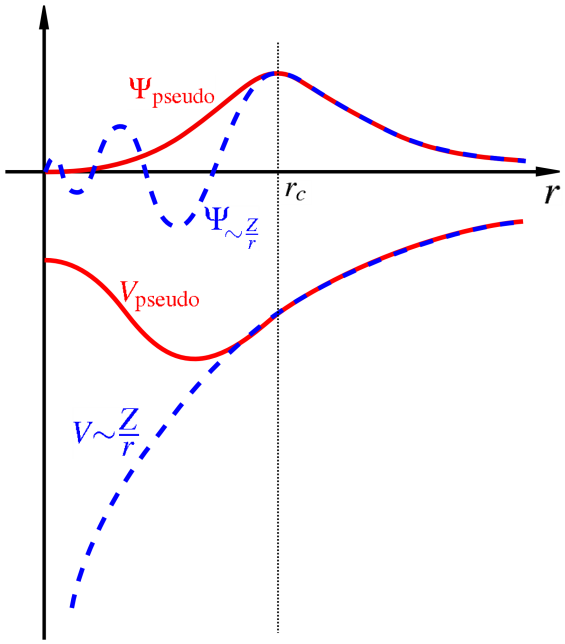

Figure 1.4: *Schematic representation of the pseudopotential and pseudo-wavefunction concepts. The blue dashed lines show the all-electron wavefuntion and the ionic potential. The red solid lines show the pseudo-wavefunction and the pseudopotential.*

1.3.8 Pseudopotentials

To overcome the problem of the high computational cost of the plane waves formulation when it comes to the region around atoms, we make use of so-called pseudopotentials. The issue in the core region of atoms is that the electronic wavefunction oscillates a lot more than in the valence region, hence the need of a large number of plane waves to describe it. Besides, generally the core electronic structure is not affected by the chemical bonds of the outer electrons, and the valence electron do not feel the complete Coulombian potential of the nuclei, but a potential screened by the core electrons. In the light of these concepts, the pseudopotential approximation replaces the strong and singular ionic potential in the core region by a weaker pseudopotential. The former and the latter are identical outside the chosen core radius r_c, as well as the all-electron wavefunction and the pseudo-wavefunction. The latter however does not feature the oscillation from the former as pictured in Fig. 1.4.

Any valid pseudopotential must fulfill the following conditions :

- for $r > r_c$, the pseudopotential and the original potential must be identical
- for $r > r_c$, the valence pseudo-wavefunction is the same than the one obtained for a reference configuration of the chosen atom
- for $r < r_c$, the pseudo-wavefunction must not have any node
- the valence states of the pseudo-atom must be equal to the ones obtained from the resolution of the Schrödinger equation for the real atom.

1.3.9 Structure optimization

To obtain accurate results for phonon calculations and all other properties of a system, its crystalline structure must be stable. To obtain the optimal stability, we need to compute the forces acting on the atoms and the stress and strain applied on unit cells. The application of strain changes the shape of the unit cell. If we define a matrix $\mathbf{h}$ with columns the unit cell vector $\mathbf{a}, \mathbf{b}, \mathbf{c}$, then the unit cell shape change is :

$$\mathbf{h}' = (\mathbb{1} + \epsilon)\mathbf{h} \tag{1.13}$$

where ϵ is the strain tensor. The stress tensor is given by :

$$\sigma_{\alpha\beta} = \frac{1}{\Omega}\frac{\partial E}{\partial \epsilon_{\alpha\beta}} \tag{1.14}$$

where $\Omega = \mathbf{a} \cdot (\mathbf{b} \times \mathbf{c})$ is the volume of the unit cell, α, β are the angles in the unit cell.
To compute all of this, we could compute the derivative of the total energy by finite differences, *ie.* by computing it at several points around the point of interest and do a numerical derivative but the computational cost would be too high. Instead, we use perturbation theory *via* the Hellman-Feynman theorem. Classically, a force is the derivative of the potential energy :

$$\mathbf{F} = -\nabla_{\mathbf{R}} U(\mathbf{R})$$

The quantum mechanical equivalent would be :

$$\mathbf{F} = -\nabla_{\mathbf{R}} \langle E \rangle$$

where $\langle E \rangle = \langle \Psi | H | \Psi \rangle$, if the $|\Psi\rangle$ are normalized. We have :

$$\frac{\partial\langle E\rangle}{\partial\lambda} = \left\langle \tfrac{\partial\Psi}{\partial\lambda}\right| H\left|\Psi\right\rangle + \left\langle\Psi\right| \tfrac{\partial H}{\partial\lambda}\left|\Psi\right\rangle + \left\langle\Psi\right| H \left|\tfrac{\partial\psi}{\partial\lambda}\right\rangle$$

The $|\Psi\rangle$ are solutions of the Schrödinger equation so we have $H|\Psi\rangle = E|\Psi\rangle$, therefore :

$$\frac{\partial\langle E\rangle}{\partial\lambda} = \langle\Psi| \frac{\partial H}{\partial\lambda}|\Psi\rangle. \tag{1.15}$$

This last equation is known as the Hellman-Feynman theorem. With the plane waves basis we chose earlier in section 1.3.6, which is independent of the ionic coordinates, we have :

$$|\Psi\rangle = \sum_j c_j |\phi_j\rangle$$

where ϕ is a plane wave. The Hellman-Feynman theorem translates to :

$$\begin{aligned}\frac{\partial\langle E\rangle}{\partial R} &= \frac{\partial}{\partial R}\left\langle \sum_j c_j^*\phi_j^*(r)\right| H \left|\sum_i c_i\phi_i^*(r)\right\rangle \\ &= \sum_{i,j} c_j^* c_i \left\langle\phi_j^*(r)\right| \tfrac{\partial H}{\partial R}\left|\phi_i(r)\right\rangle .\end{aligned}$$

It means that we can calculate the force using the same coefficients c_j as we used to minimize the energy. This makes the calculation of forces easier after the energy is minimized. There are similar expressions for the stresses. To optimize the structures, one needs to minimize the forces and stresses acting on the atom and unit cells. Thanks to the Born-Oppenheimer approximation, we only need to optimize the ionic configuration and it is assumed that the electrons adapt to it instantly. The ionic positions are considered to be parameters. Finding the ground-state structure is an optimisation problem with several particularities : the phase space grows with the system size, there are local minima corresponding metastable structures and we generally need to start with a good initial guess of the structure. There exist several methods to solve the optimization problem, such as steepest descent, molecular dynamics, conjugate gradients or simulated annealing, but the code we used in this work employs the so-called Broyden-Fletcher-Goldfard-Shanno (BFGS) algorithm. Let us describe briefly the way it works.

The aim is to minimize a function f with respect to a vector x. In our case, $f(\mathbf{x}) = E(\mathbf{R})$. Before the algorithm begins we need to give it an initial estimation of the optimal value $\mathbf{x}_0$. At every stage n, the algorithm tries to obtain a better estimate for the minimum of $f(\mathbf{x})$ by searching in the direction $\mathbf{p}_n$, given by the equation :

$$B_n \mathbf{p}_n = -\nabla f(\mathbf{x}_n),$$

which is analogue to a Newton equation of motion, except that B_n is an approximation to the Hessian matrix (the matrix of second derivatives). This is why the BFGS algorithm is known as a quasi-Newton's method. This approximate matrix is updated at each iteration. To find the next estimation point $\mathbf{x}_{n+1}$, the algorithm performs a line search in the direction $\mathbf{p}_k$ such that $f(\mathbf{x}_n + \gamma \mathbf{p}_k)$ is minimal. Now we define $\mathbf{y}_n = \nabla f(\mathbf{x}_{n+1}) - \nabla f(\mathbf{x}_n)$ and $\mathbf{s}_n = \mathbf{x}_{n+1} - \mathbf{x}_n$. The condition on the update of B_n is given by :

$$B_{n+1} = B_n + \frac{\mathbf{y}_n \mathbf{y}_n^\top}{\mathbf{y}_n^\top \mathbf{s}_n} - \frac{B_n \mathbf{s}_n \mathbf{s}_n^\top B_n^\top}{\mathbf{s}_n^\top B_n \mathbf{s}_n}$$

This algorithm converges more rapidly that the other methods named above and contains physical information in the approximate Hessian. However, this matrix requires a lot of storage and the algorithm can get stuck in a local minimum, in other words a metastable structure.

1.4 Density Functional Perturbation Theory

Let us now present how the phonon modes are computed in DFT. As seen above, in order to compute the phonon modes, one need to solve the secular equation :

$$\omega^2 \epsilon_{\alpha i}(\mathbf{q}) = D_{\alpha i}^{\beta j} \epsilon_{\beta j}(\mathbf{q})$$

. The matrix D is the dynamical matrix given by the expression :

$$\det\big(\boldsymbol{D}(\mathbf{q}) - \omega^2 \mathbb{1}\big) = 0$$

where $\boldsymbol{D}$ is the dynamical matrix given by :

$$D_\alpha^\beta = \frac{1}{\sqrt{M_\alpha M_\beta}} \frac{\partial^2 E_{tot}(\mathbf{R})}{\partial \mathbf{R}_\alpha \partial \mathbf{R}_\beta}.$$

The matrix of second derivatives of the total energies is called the Hessian matrix, or the matrix of the interatomic force constants. It is proportional to the electronic density response to a distortion of the lattice geometry.

$$\frac{\partial^2 E_{tot}(\mathbf{R})}{\partial \mathbf{R}_\alpha \partial \mathbf{R}_\beta} = \int \frac{\partial n_0(\mathbf{r})}{\partial \mathbf{R}_\beta} \frac{\partial V_{eN}(\mathbf{r})}{\partial \mathbf{R}_\alpha} d\mathbf{r} + \int n_0(\mathbf{r}) \frac{\partial^2 V_{eN}}{\partial \mathbf{R}_\alpha \mathbf{R}_\beta} d\mathbf{r} + \frac{\partial V_{ext}(\mathbf{R})}{\partial \mathbf{R}_\alpha \partial \mathbf{R}_\beta}$$

where n_0, V_{eN}, V_{ext} are respectively the ground state density, the electron-ion interaction potential and the external potential acting on electrons. To be more general, we give the expression of the Hessian with respect to a set of parameters $\lambda = \{\lambda_i\}$. In the case of lattice dynamics, we would have $\lambda_i = R_\alpha$:

$$\frac{\partial^2 E}{\partial \lambda_i \partial \lambda_j} = \int \frac{\partial n_\lambda(\mathbf{r})}{\partial \lambda_j} \frac{\partial V_\lambda(\mathbf{r})}{\partial \lambda_i} d\mathbf{r} + \int n_\lambda(\mathbf{r}) \frac{\partial^2 V_\lambda}{\partial \lambda_i \partial \lambda_j} d\mathbf{r}.$$

The density is given by :

$$n(\mathbf{r}) = 2 \sum_{i=1}^{N/2} |\varphi_i(\mathbf{r})|^2 \tag{1.16}$$

where φ_i is an eigenfunction of the Kohn-Sham equations :

$$\left(-\frac{\hbar^2}{2m} \boldsymbol{\nabla}_\mathbf{r} + V_{KS}(\mathbf{r}) \right) \varphi_i(\mathbf{r}) = \varepsilon_i \varphi_i(\mathbf{r})$$

and V_{KS} is the Kohn-Sham potential. The density can be obtained by linearizing Eq. 1.16 :

$$\Delta n(\mathbf{r}) = 4 \,\mathrm{Re} \sum_{i=1}^{N/2} \varphi_i^*(\mathbf{r}) \Delta \varphi_i(\mathbf{r}), \tag{1.17}$$

where the finite difference operator Δ^λ of any function F is defined as :

$$\Delta^\lambda = \sum_i \frac{\partial F_\lambda}{\partial \lambda_i} \Delta \lambda_i$$

The superscript λ is omitted when there is no ambiguity. Since the external potential is real, the Kohn-Sham eigenfunctions and their complex conjugate are degenerate, hence the imaginary part of the sum in equation 1.17 vanishes. The variation of the Kohn-Sham orbitals $\Delta\varphi_i(\mathbf{r})$ is given by the first order perturbation theory, known as the Sternheimer equation :

$$(H_{KS} - \varepsilon_i) |\Delta \varphi_i\rangle = - (\Delta V_{KS} - \Delta \varepsilon_i) |\varphi_i\rangle \tag{1.18}$$

where

$$H_{KS} = \frac{\hbar^2}{2m} \boldsymbol{\nabla}_{\boldsymbol{r}} + V_{KS}(\mathbf{r})$$

is the unperturbed Hamiltonian. The first order correction to the Kohn-Sham potential is ;

$$\Delta V_{KS}(\mathbf{r}) = \Delta V_{ext}(\mathbf{r}) + e^2 \int \frac{\Delta n(\mathbf{r}')}{|\mathbf{r}-\mathbf{r}'|} d\mathbf{r}' + \frac{\partial v_{xc}(n)}{dn}\Big|_{n=n(\mathbf{r})} \Delta n(\mathbf{r})$$

and the first order variation of the Kohn-Sham eigenvalue is $\Delta\varepsilon_i = \langle\varphi_i| \Delta V_{KS} |\varphi_i\rangle$.

This is still a self-consistent problem since $\Delta V_{KS}(\mathbf{r})$ is a linear functional of $\Delta n(\mathbf{r})$ which in turn depends linearly on the $\Delta\varphi$'s. It has become a generalized linear problem, with N linearly coupled equations. Indeed, Δn depends on all the solutions $\Delta\varphi_j$ $(j \neq i)$ of the equations similar to Eq. 1.18.

We can also express an eigenfunction in terms of a sum over the spectrum of the unperturbed Hamiltonian :

$$\Delta\varphi_i(\mathbf{r}) = \sum_{j\neq i} \varphi_j(\mathbf{r}) \frac{\langle\varphi_j| \Delta V_{KS} |\varphi_i\rangle}{\varepsilon_i - \varepsilon_j} \tag{1.19}$$

with a sum running over all the occupied and empty states. The density response becomes :

$$\Delta n(\mathbf{r}) = 4 \sum_{i=1}^{N/2} \sum_{j\neq i} \varphi_i^*(\mathbf{r})\varphi_j(\mathbf{r}) \frac{\langle\varphi_j| \Delta V_{KS} |\varphi_i\rangle}{\varepsilon_i - \varepsilon_j}. \tag{1.20}$$

It can be seen from this equation that the contribution coming from products of occupied states (for $j \leq N/2$) cancel each other, by inversion of i and j. This is equivalent to say that the density does not respond to a perturbation acting only the set of occupied states.

The evaluation of $\Delta\varphi_i(\mathbf{r})$ from Eq. 1.19 requires the knowledge of the full spectrum of H_{KS}, even unoccupied conduction states. However, in Eq. 1.18, only the knowledge of the occupied states is needed to construct the right hand side of the equation, and one can use iterative algorithm to solve the linear system. Therefore the computational cost of determining the density response to a single perturbation is of the same order as the calculation of the unperturbed ground state density. In this work, we use DFPT to compute the phonon modes, atomic vibrations being considered as perturbation of the crystal structure.

Chapter 2

Phonons and electron-phonon coupling

2.1 Electron-phonon coupling from finite differences

Once we computed the electronic properties of our systems and their phonon modes, we could start computing the electron-phonon interaction, which we present in this section.

We are interested in the thermal average of an electronic operator at a given temperature T. The operator is averaged over special configurations that depend on the atomic vibrations. In our formalism we define the electron-phonon interaction as the change of electronic operator due to the atomic displacement. In the scientific literature there are two ways to compute the electron-phonon interaction on a given property.

The first is by finite differences, which we used in this work. It consists of moving explicitly the atoms to the desired configurations and perform the electronic response to the displacement. The shortcoming of finite displacement is that in order to describe long wavelengths, we need to have large supercells and this is a computational bottleneck. The advantages of this method are that we can use any method to compute the electronic states, since we only need to be compute properties at given atomic configurations. Also, the finite differences account for terms in the electron-phonon interaction beyond the first order.

The other method is to use linear response in DFPT to an atomic displacement in the primitive unit

cell. The advantage is that it requires only one unit cell, which amounts to a smaller computational cost. The shortcomings of this method is that it can only be used in semi-local DFT (with the use of the LDA and likewise approximations), and that we can not account for higher terms after the lowest in the electron-phonon interaction. Depending on the characteristics of the system studied, one can chose the best-suited approach.

Recent developments have made finite difference methods much more efficient. An example is the use of Monte-Carlo sampling to compute the thermal average only on certain selected configurations [8], reducing the size of the phase-space. Another technique is the use of non-diagonal supercells, which also decrease the number of degrees of freedom of the system, speeding up the calculations [34]. In the following section, we present the derivation of the thermal line approach or special displacement configuration, that allow to calculate the average of an operator with a small number of configurations or even a single-one.

2.1.1 Thermal average of an operator at temperature T=0

Let $\hat{A}$ be an operator. We set ourselves in the harmonic approximation *ie.* the ground state is approximated to a quantum harmonic oscillator. Let $|\psi_0\rangle$ be the fundamental state of the harmonic oscillator. We want to compute the average of $\hat{A}$ ie $\langle\psi_0|\hat{A}|\psi_0\rangle$. Let x be a one dimensional space variable that could represent for example the phonons amplitude. In space representation the wave function of the fundamental state is :

$$\psi_0(x) = \left(\frac{m\omega_0}{\pi\hbar}\right)^{1/4} \exp\left(-\frac{m\omega_0}{2\hbar}x^2\right).$$

Now we have :

$$\langle\psi_0|\hat{A}|\psi_0\rangle = \left(\frac{m\omega_0}{\pi\hbar}\right)^{1/2} \int_{-\infty}^{+\infty} dx \exp\left(-\frac{m\omega_0}{2\hbar}x^2\right) \hat{A}(x). \tag{2.1}$$

In order to compute this integral we expand $\hat{A}$ around $x = 0$:

$$\hat{A}(x) = \hat{A}(0) + x\frac{\partial\hat{A}}{\partial x}\Big|_{x=0} + \frac{1}{2}x^2\frac{\partial^2\hat{A}}{\partial x^2}\Big|_{x=0} + \mathcal{O}(x^3) \tag{2.2}$$

And we plug it in the integral (2.1). The term linear (as all the odd power terms) in x will vanish because it is multiplied by an even function in the integrand. We drop the term corresponding to the integration of $\hat{A}(0)$ because it is a constant, and we are left with :

$$\begin{aligned}\langle\psi_0|\hat{A}|\psi_0\rangle &= \left(\frac{m\omega_0}{\pi\hbar}\right)^{1/2}\frac{\partial^2\hat{A}}{\partial x^2}\Big|_{x=0}\int_{-\infty}^{+\infty}dx x^2\exp\left(-\frac{m\omega_0}{2\hbar}x^2\right)+... \\ &= \frac{1}{2}\frac{\hbar}{m\omega_0}\frac{\partial^2\hat{A}}{\partial x^2}\Big|_{x=0}\end{aligned}$$

Now if we assume the operator is purely quadratic *i.e* $\hat{A} = \frac{1}{2}x^2\frac{\partial^2\hat{A}}{\partial x^2}\Big|_{x=0}$, then there exists a value of x^* for which $\langle\psi_0|\hat{A}|\psi_0\rangle = \hat{A}(x^*)$. Some simple math gives:

$$x^* = \pm\sqrt{\frac{\hbar}{m\omega_0}} \tag{2.3}$$

This result shows that in harmonic approximation it is possible to calculate the average of an operator using a single atomic configuration. The result of the present section can be easily generalized to more dimensions. In the next section we will extend the formula Eq. 2.3 to finite temperature.

2.1.2 Average value of an operator at finite temperature T

In general at finite temperature T, the average of an operator in the canonical ensemble writes :

$$\left\langle\hat{A}(T)\right\rangle = \frac{1}{\mathcal{Z}}\sum_n\langle E_n|\,\hat{A}\,|E_n\rangle\,e^{-\frac{E_n}{k_BT}}$$

where E_n is the energy associated with the eigenstate $|E_n\rangle$, $\mathcal{Z} = \sum_n e^{-\frac{E_n}{k_BT}}$ is the partition function and k_B is the Boltzmann constant. We will compute the average of an operator A at finite temperature on an harmonic oscillator configurations, who are defined as :

$$\psi_n(x) = \frac{1}{\sqrt{2^n n!}}\left(\frac{m\omega}{\pi\hbar}\right)^{1/4}e^{-\frac{m\omega}{2\hbar}x^2}H_n\left(\sqrt{\frac{m\omega}{\hbar}}x\right)$$

where H_n is the Hermite polynomial of order n. The energies associated with the eigenstates are :

$$E_n = \hbar\omega\left(n+\frac{1}{2}\right)$$

Using these, the average of operator $\hat{A}$ writes :

$$\left\langle\hat{A}(T)\right\rangle = \frac{1}{\mathcal{Z}}\sum_n e^{-\frac{\hbar\omega(n+1/2)}{k_BT}}\frac{1}{2^n n!}\int_{-\infty}^{+\infty}dx\sqrt{\frac{m\omega}{\pi\hbar}}\hat{A}(x)e^{-\frac{m\omega}{\hbar}x^2}H_n^2\left(\sqrt{\frac{m\omega}{\hbar}}x\right)$$

We do the change of variable $\sqrt{\frac{m\omega}{\hbar}}x = y$, so

$$\left\langle \hat{A}(T) \right\rangle = \frac{1}{\mathcal{Z}} \sum_n \frac{e^{-\frac{\hbar\omega(n+1/2)}{k_B T}}}{2^n n! \sqrt{\pi}} \int_{-\infty}^{+\infty} dy \hat{A} \left(\sqrt{\frac{\hbar}{m\omega}} y \right) e^{-y^2} H_n^2(y) \tag{2.4}$$

We compute it using the same kind of expansion than in (2.2). The operator assumes the same expansion both in x and y because the relation between the two variables is linear. Once again we will not keep the term in $\hat{A}(0)$ because it is just a constant. The term linear in y gives the following integral :

$$\frac{\partial \hat{A}}{\partial y}\Big|_{y=0} \int_{-\infty}^{+\infty} dy \; y H_n^2(y) e^{-y^2} \tag{2.5}$$

We use the following properties of the Hermite polynomials :

$$y H_n(y) = \frac{1}{2} H_{n+1}(y) + n H_{n-1}(y) \tag{2.6}$$

$$\implies y H_n^2(y) = \frac{1}{2} H_{n+1}(y) H_n(y) + n H_{n-1}(y) H_n(y) \tag{2.7}$$

and

$$\int_{-\infty}^{+\infty} dx H_n(x) H_m(x) e^{-x^2} = 2^n n! \sqrt{\pi} \delta_{n,m} \tag{2.8}$$

Finally the term linear in y of (2.5) vanishes using (2.7) and (2.8). To compute the term in y^2, we use the same property than in (2.7) :

$$y^2 H_n^2(y) = \frac{1}{4} H_{n+1}^2(y) + n^2 H_{n-1}^2(y) + n H_{n+1}(y) H_{n-1}(y) \tag{2.9}$$

The term in y^2 in (2.4) becomes, making use of (2.8) and (2.9) :

$$\frac{1}{2} \frac{\partial^2 \hat{A}}{\partial y^2}\Big|_{y=0} \int_{-\infty}^{+\infty} dy \; y^2 H_n^2(y) e^{-y^2} = \frac{1}{2} \frac{\partial^2 \hat{A}}{\partial y^2}\Big|_{y=0} \sqrt{\pi} 2^n n! \left(n + \frac{1}{2} \right)$$

Equation (2.4) becomes :

$$\left\langle \hat{A}(T) \right\rangle = \frac{1}{2} \frac{\partial^2 \hat{A}}{\partial y^2}\Big|_{y=0} \frac{1}{\mathcal{Z}} \sum_n e^{-\frac{\hbar\omega(n+1/2)}{k_B T}} \left(n + \frac{1}{2} \right) \tag{2.10}$$

Now we take a look at the partition function $\mathcal{Z}$ in the case of the harmonic oscillator :

$$\frac{1}{\mathcal{Z}} = \frac{1}{\sum_n e^{-\frac{\hbar\omega\left(n+\frac{1}{2}\right)}{k_B T}}} = e^{\frac{\hbar\omega}{2k_B T}} \left(1 - e^{-\frac{\hbar\omega}{k_B T}} \right),$$

by properties of the geometric series. The latter also give the result :

$$\sum_n e^{-\frac{\hbar\omega(n+1/2)}{k_B T}} \left(n+\frac{1}{2}\right) = e^{-\frac{\hbar\omega}{2k_B T}} \left[\frac{1}{2\left(1-e^{-\frac{\hbar\omega}{k_B T}}\right)} + \frac{e^{-\frac{\hbar\omega}{k_B T}}}{\left(1-e^{-\frac{\hbar\omega}{k_B T}}\right)^2}\right]$$

If we come back to the original variable x with $\frac{\partial^2 \hat{A}}{\partial y^2} = \frac{\hbar}{m\omega}\frac{\partial^2 \hat{A}}{\partial x^2}$, the average of operator $\hat{A}$ is given by :

$$\left\langle \hat{A}(T) \right\rangle = \frac{\hbar}{2m\omega}\frac{\partial^2 \hat{A}}{\partial y^2}\Big|_{y=0} \left(\frac{1}{2} + n_B(\omega, T)\right),$$

where $n_B(\omega, T) = (e^{\hbar\omega/k_B T} - 1)^{-1}$ is the Bose-Einstein function. Similarly than in the previous section, we would like to find a value x^* for which $\left\langle \hat{A}(T) \right\rangle = \hat{A}(x^*)$. If we assume $\hat{A}$ to be purely quadratic, *i.e* $\hat{A}(x) = \frac{1}{2}\frac{\partial^2 \hat{A}}{\partial x^2}\Big|_{x=0}$, then

$$x^*(T) = \pm\sqrt{\frac{\hbar}{m\omega}\left(\frac{1}{2} + n_B(\omega, T)\right)}$$

The plus and minus solutions are the two equivalent displacements that give the average of the operator at finite temperature. In a real system, in harmonic approximation all the vibrational modes are independent. Therefore we can displace all atoms from the equilibrium configuration to a special configuration by displacing all of them at once by a general displacement. We define the general displacement to be the sum of all the individual atom displacements along the eigenmodes of vibration ϵ_ν :

$$\Delta r_{sa} = \sum_\nu S_\nu \sqrt{\frac{\hbar}{m_s\omega_\nu}} \sqrt{1 + 2n_B(\omega_\nu, T)}\ \epsilon_{sa,\nu} \tag{2.11}$$

where s and a denote respectively for an atom and a cartesian coordinate. The coefficient S_ν is either + or -. Since for each vibrational mode there are two possible solution that give that same average, in a system with P vibrational modes we will have 2^P possibilities to generate this general displacement, that are 2^P sign combinations of the coefficients in equation 2.11.

In their article [9] Zacharias and Giustino proposed the following formula for the general displacement Δr_{sa} :

$$\Delta r_{sa} = \sum_\nu (-1)^{\nu-1} \sqrt{\frac{\hbar}{m_s\omega_\nu}} \sqrt{1 + 2n_B(\omega_\nu, T)}\ \epsilon_{sa,\nu}, \tag{2.12}$$

They show that the plus and minus sign alternation in the sum of equation 2.12 reduces the numerical error in the limit of large supercells. This is one choice of sign combination. We refer to this configuration later as *ZG displacement*.

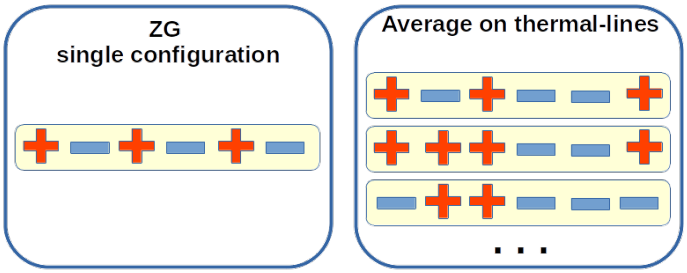

Figure 2.1: *Different choices of sign combination in the sum of equation 2.11*

Another choice was made by Monserrat in ref [8]. He calls *thermal line* the configuration arising from a general displacement with a unique sign combination for the S_ν's in the sum 2.11. His approach is to average over a subset of all the thermal lines *ie.* averaging over several special configurations, selecting them with a Monte-Carlo method. This is supposed to yield more precise results even in small supercells, but it is slower to converge since it requires one DFPT calculation per thermal line. A sketch of the different choices of sign combination is shown in figure 2.1. We have tested both methods and chosen the one best-suited to our needs (see section 3.2).

2.2 Mapping of phonons to a supercell

As seen above, we need to compute the electronic properties by finite displacements in supercells to account for long wavelength vibrations. However the computation of phonons in supercells is highly time consuming. Hence we use the following method to map phonons computed in a unit cell to supercells of any size. We follow the notation of Ashcroft-Mermin Chapt. 22 [21] and write the solutions of the harmonic problem in periodic systems within the Born-von Karman boundary conditions as:

$$u_\mu(\mathbf{q}, t) = \epsilon_\mu e^{i(\mathbf{q}\cdot\mathbf{R} - \omega^\mu_\mathbf{q} t)} \tag{2.13}$$

where the complex eigenvectors ϵ_μ of the dynamical matrix are calculated by means of DFTP, $\mathbf{q}$ is a regular point grid in the first Brillouin zone, and $\omega^\mu_\mathbf{q}$ are the eigenvalues. For unit cells with

p atoms, the number of eigenvectors is $3p$, and their length is also $3p$. Suppose we have a regular grid of q-points (n_{qx}, n_{qy}, n_{qz}) for a total of $n_{\mathbf{q}} = n_{qx} \cdot n_{qy} \cdot n_{qz}$.

A phonon mode computed in a unit cell at a given **q**-point can be mapped in a supercell of size (n_{qx}, n_{qy}, n_{qz}), at the center of the supercell in reciprocal space. Care should be taken about the order of the new eigenvalues and eigenvectors $\tilde{\omega}, \tilde{\epsilon}$, for they are obtained with the old eigenvalues and eigenvectors computed on the **q**-grid. For this, we associate each subcell of the supercell to a unique **q**-point in the grid, as sketched in figure 2.2.

In order to map the phonons first of all we construct the new eigenvalues and eigenvectors $\tilde{\omega}, \tilde{\epsilon}$. The eigenvalues can be easily constructed as:

$$\tilde{\omega} = \begin{pmatrix} \omega_{q_1} \\ \omega_{q_2} \\ \vdots \\ \omega_{q_{n\mathbf{q}}} \end{pmatrix}$$

At each **q**-point, we obtained $3p$ eigenvalues. They are all ordered and associated with a new eigenvector.

For the new eigenvectors we divide the procedure in two steps. First we construct eigenvectors without phase correction just by concatenating the old eigenvectors components such as :

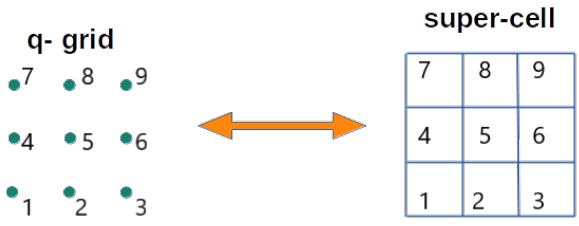

Figure 2.2: *Sketch of the correspondence between a **q**-point and a subcell of 3x3 supercell.*

$$\tilde{\epsilon}_{\mu+\mathbf{q}_1} = \begin{pmatrix} \epsilon^{\mu}_{\mathbf{q}_1} \\ \epsilon^{\mu}_{\mathbf{q}_1} \\ \vdots \\ \epsilon^{\mu}_{\mathbf{q}_1} \end{pmatrix}, ..., \tilde{\epsilon}_{\nu+\mathbf{q}_2} = \begin{pmatrix} \epsilon^{\nu}_{\mathbf{q}_2} \\ \epsilon^{\nu}_{\mathbf{q}_2} \\ \vdots \\ \epsilon^{\nu}_{\mathbf{q}_2} \end{pmatrix}$$

where the vectors $\epsilon^{\mu}_{\mathbf{q}}$ are defined in the unit cell and they have the dimension of $3p$ while the vectors $\tilde{\epsilon}_{\mu}$ are in the supercell and they have dimension $(3 \cdot N \cdot n_{\mathbf{q}})$. In the unit cell there are $3p$ eigenvectors for each q-point, while in the supercell there are $3pn_{\mathbf{q}}$ for a single q-point, the same number in both cases. Notice that we have copied the same eigenvector for each of the cell that compose the supercell. Now we have have to apply the phase factor of equation 2.13 as:

$$\tilde{\epsilon}_{\mu+\mathbf{q}_1} = \begin{pmatrix} \epsilon^{\mu}_{\mathbf{q}_1} \cdot e^{i\mathbf{q}_1 R_1} \\ \epsilon^{\mu}_{\mathbf{q}_1} \cdot e^{i\mathbf{q}_1 R_2} \\ \vdots \\ \epsilon^{\mu}_{\mathbf{q}_1} \cdot e^{i\mathbf{q}_1 R_N} \end{pmatrix}$$

where the R_N are the translation vectors that generate the different cells that form the supercell, starting from the unit cell. In the part care should be taken because the order of the cells must be the same for the atomic structure and polarization vectors. Finally, since there is an arbitrarity in the choice of the eigenvector phase, we can consider only the real-part of these vectors.

$$\tilde{\epsilon}_{\mu+\mathbf{q}_1} = \begin{pmatrix} Re\left[\epsilon^{\mu}_{\mathbf{q}_1} \cdot e^{i\mathbf{q}_1 R_1}\right] \\ Re\left[\epsilon^{\mu}_{\mathbf{q}_1} \cdot e^{i\mathbf{q}_1 R_2}\right] \\ \vdots \\ Re\left[\epsilon^{\mu}_{\mathbf{q}_1} \cdot e^{i\mathbf{q}_1 R_N}\right] \end{pmatrix}$$

This approach speed up a lot our simulations, because we only need a single converged DFTP calculation in the unit cell, then we can interpolate phonon modes using Fourier transform to any grid of **q**-points and map them to the desired supercell, instead of computing the phonons with DFPT in every supercell. This greatly speeds up the computation process, since DFPT computation of phonons requires a number of plane waves scaling with the cube of the number of atoms in the system.

Chapter 3

Systems and Results

3.1 Materials

Now we present the materials to which we applied the theory developed in the previous chapter. Each material was chosen for a different reason: Polyethylene is a one-dimensional system, and therefore convergence with the supercell is faster; hexagonal Boron Nitride in bulk has a strong electron-phonon coupling; Phosphorene that is a non-polar material and therefore converge is expected to be faster with the supercell.

3.1.1 Polyethylene

We chose to test our methods on polyethylene, a linear polymer, to verify the convergence of the phonon mapping and finite displacement averages with a relatively low computational time. Polyethylene is an insulating polymer whose monomers are ethylenes, organic molecules composed of carbon and hydrogen. We optimized the atom positions in the unit cell shown in figure 3.1 in DFT as explained in section 1.3.9.

We used a 18x1x1 **k**-points grid and a norm-conserving pseudopotential using a GGA exchange-correlation functional (PBE) from the PseudoDojo project [35] to obtain the optimized equilibrium geometry.

Polyethylene is an insulating material with a measured band gap of 8.8 eV. We display its electronic band structure in figure 3.2. This was computed in DFT and we can clearly see the underestimation

of the band gap, a well-known problem of DFT.

The phonon dispersion of polyethylene is shown in figure 3.3. We can see that there are a lot of non-degenerate branches at the Γ point. This is due partially to the number of atoms in a single unit cell equal to 6, and also to the fact that the polyethylene being constituted of 2 different atoms, and so there is a breaking of transverse and longitudinal optical modes at Γ point.

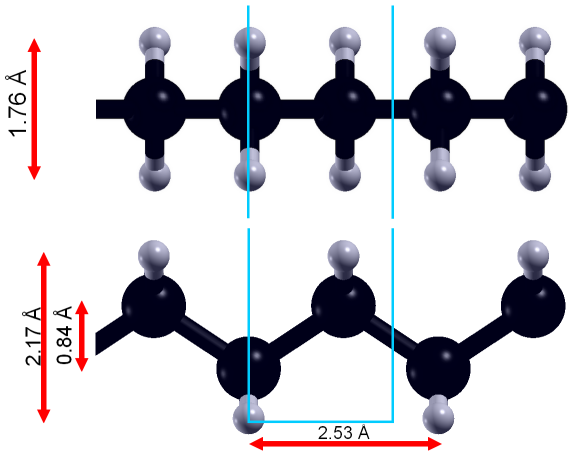

Figure 3.1: *Top view (top) and side view (bottom) of the optimized geometry of polyethylene, with the orthorombic unit cell.*

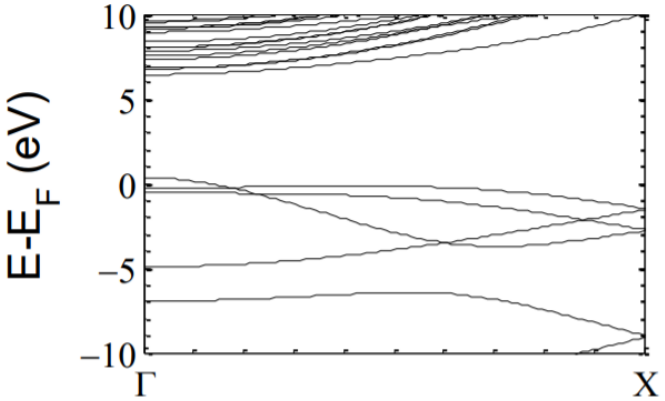

Figure 3.2: *Electronic band structure of polyethylene. Image taken from [36].*

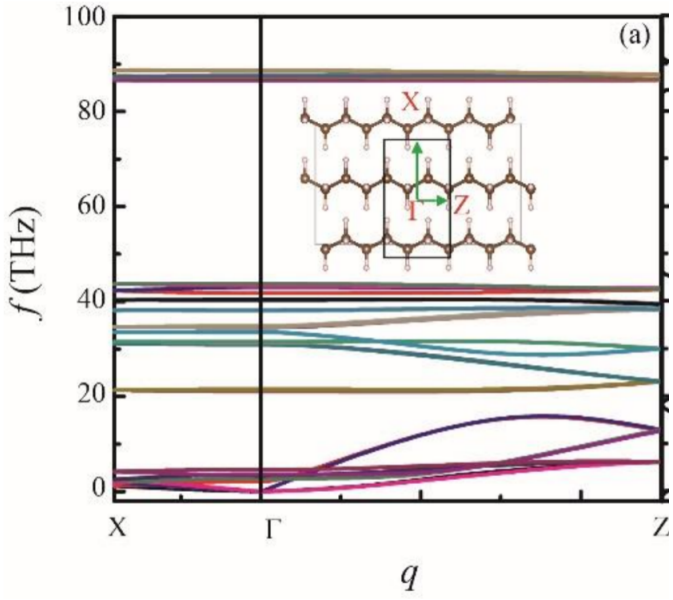

Figure 3.3: *Phonon dispersion of polyethylene. Image taken from [37].*

3.1.2 Hexagonal Boron Nitride

The second material we investigated is monolayered hexagonal Boron Nitride. Its structure is similar to the one of graphene but with polar B-N bonds, and its electronic and optical properties make it an interesting material in the light of Van der Waals heterostructures. Its structure is displayed in figure 3.4. We used a 15x15x1 **k**-point grid and a norm conserving pseudopotential with a GGA exchange-correlation functional to optimize its geometry.

It is a wide band gap semi-conductor with a direct gap of 5.76 eV and an indirect gap of 5.955 eV [38]. Its electronic structure is displayed is figure 3.5. It has been computed in DFT and once again we can see that the gap in underestimated. There has been a debate in literature on whether the nature of hexagonal Boron Nitride's band gap. It comes from the contrast between *ab initio* simulations predicting an indirect band gap [39, 40], whereas optical experiment pleads in favor of a direct band gap [41]. It was later shown that the optical properties of hexagonal Boron Nitride where largely influenced by phonon-assisted transitions [38, 42]. This has motivated the search for new theoretical tools to describe electron-phonon interactions.

The phonon dispersion of monolayered hexagonal Boron Nitride is shown in figure 3.6. Here we can see a large splitting of the transverse and longitudinal optical modes at Γ. This is the same

argument than presented previously for polyethylene, with the addition that, the B-N bond being polar, a vibration produces an electric dipole which creates long-range electric fields. This long range Coulomb interaction between dipoles affects the longitudinal and transverse optical modes differently, which leads to a difference in the energy they bring to the crystal by vibrating, hence

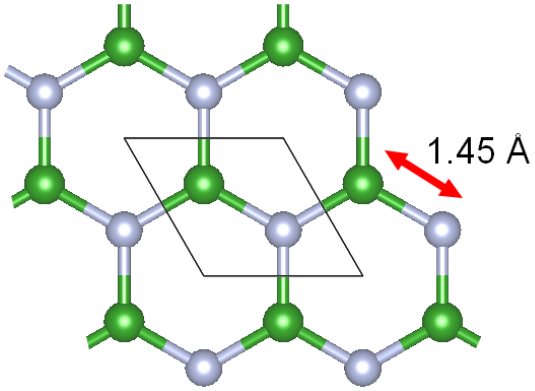

Figure 3.4: *Hexagonal Boron Nitride structure, with the diamond unit cell of simulation typical of hexagonal structures.*

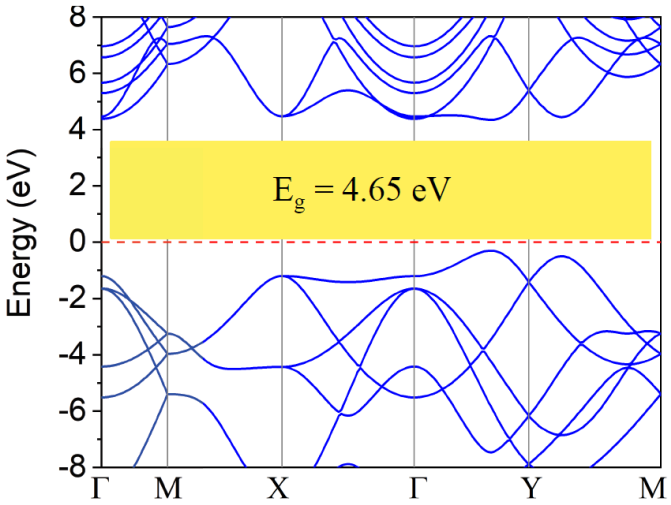

Figure 3.5: *Electronic band structure of hexagonal Boron Nitride. Image taken from [43].*

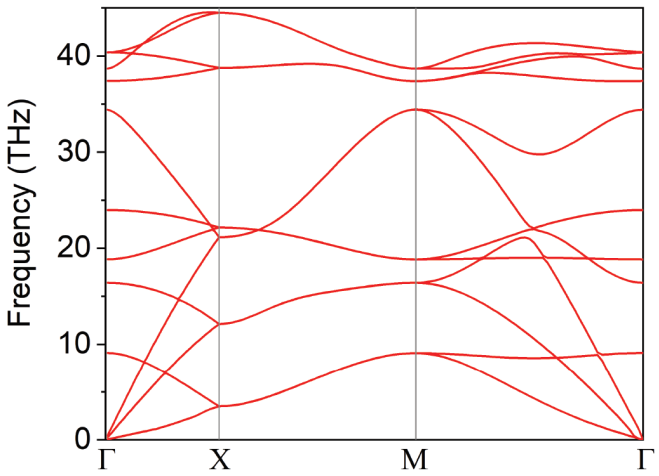

Figure 3.6: *Phonon dispersion in monolayered hexagonal Boron Nitride. Image taken from [43].*

the splitting in the phonon dispersion.

3.1.3 Phosphorene

The third material we chose to investigate is Phosphorene in the so-called α-phase. This is a monolayer semi-conductor, created by exfoliation of bulk Black Phosphorus for the first time in 2014 [44]. It has a puckered hexagonal structure, as shown in figure 3.7. The optimized equilibrium structure was computed in DFT using a 15x15x1 **k**-point grid, and a normconserving pseudopotential with a GGA exchange-correlation functional (PBE) from the PseudoDojo project.

Its structure makes it a material of choice in the construction of Van der Waals heterostructures, as well as its transport properties and its band gap of 1.88 eV [45]. This band gap is in a range of gap values where others semi-conductors are rare. We show its electronic band structure in figure 3.8.

We show the phonon dispersion of Phosphorene in figure 3.9. We chose this material because it is composed of a single element. This should limit the creation of electric dipoles due to the oscillation of polar bonds.

3.2 Gap renormalization

The first observable we decided to investigate using finite difference displacement was the DFT band gap. The results we present are the differences of the band gap values between the equilibrium structures and the special configurations we obtained from thermal average in section 2.1, for different supercell sizes. Even if the band gaps are underestimated in DFT, we can still check for the convergence of our methods with respect to sueprcell sizes. We expect the corrections to converge for large supercells, since phonons with longer and longer wavelengths are accounted for.

We first present the results of the tests we performed with polyethylene. The aim was to determine which choice of sign combination in equation 2.11 we would use, between the thermal lines from Monserrat or the Zacharias-Giustino displacement, and also to see the effect of phonon mapping on the results. Table 3.1 shows the results for the gap correction of polyethylene. We present the gap correction with respect to the size of the supercells used. Figure 3.10 displays a comparative plot of these results. The corrections from thermal lines (labelled TL in the plot) were obtained averaging over 20 lines, that are 20 different configurations. On the contrary, the correction from Zacharias-Giustino displacement (labelled ZG in the plot) is obtained only on one

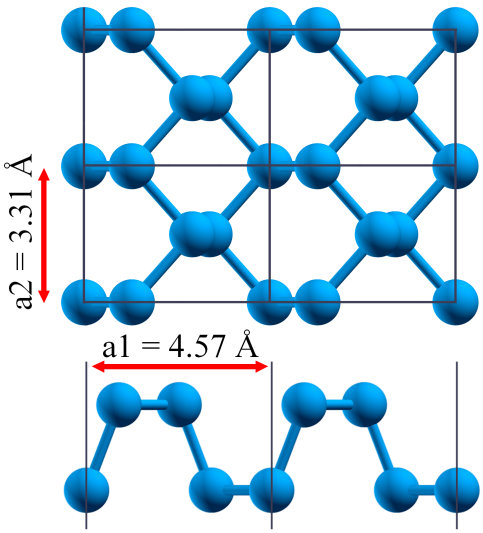

Figure 3.7: *Equilibrium structure of Phosphorene, with the unit cells of simulation. Top view (top) and side view (bottom).*

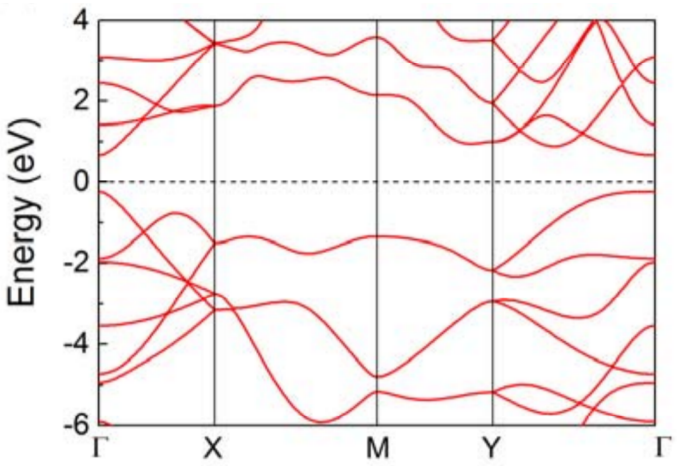

Figure 3.8: *Electronic band structure of Phosphorene. Image taken from [46].*

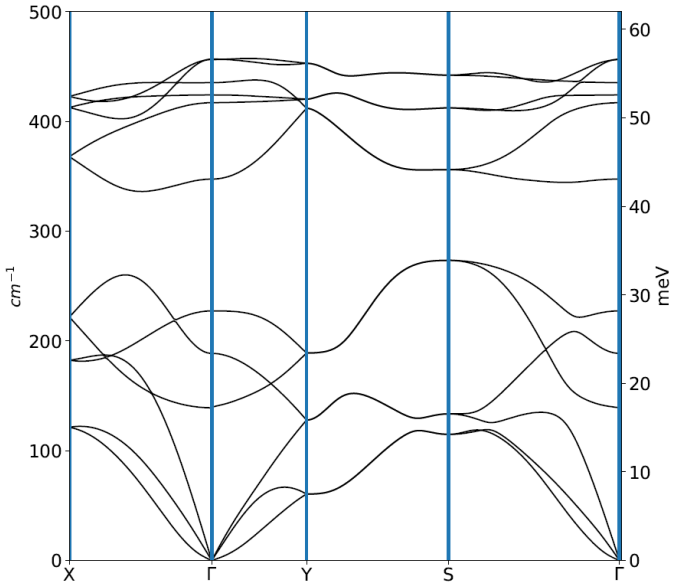

Figure 3.9: *Phonon dispersion in Phosphorene.*

configuration. For both these methods, the phonons were computed on the corresponding supercells with DFPT. For the two other methods labelled *TL mapping* and *ZG mapping*, the phonons were computed using the mapping of phonons presented in section 2.2, first computed in a unit cell with DFPT and then extrapolated to the different supercells.

The first observation we can make is that the convergence seems smoother for the thermal lines methods than for the ZG displacement methods. This is explained by the fact that the corrections obtained with the thermal lines are averaged over 20 configurations, which makes it way less sensible to numerical error that the computation with the unique configuration from ZG displacement. The second observation is that for thermal lines, the corrections are smaller when using the mapped phonons. This may be a combined numerical error from the average over the 20 configurations using the same extrapolated phonons for the five supercells. The third observations is that the corrections for larger supercells tend to converge toward the same value, except for the thermal lines with mapped phonon method. This seems to confirm the statement from Zacharias and Giustino that the ZG displacement would be more accurate with larger supercells. Finally, we decided to use the ZG displacement with mapping of phonons, since it seems to converge the same value and its computational time is the smallest of the four methods. Indeed, it only requires one DFPT computation to obtain the phonons, and one self-consistent DFT computation on the special configuration obtained with the displacement of atoms from the equilibrium configuration given by (2.12).

Unfortunately we were not able to reach convergence of the gap correction for all materials. As explained in the above section, the presence of polar bonds in polyethylene and hexagonal Boron Nitride creates electric dipoles. When we displace the atoms to the special configurations, the dipoles create long range dipole forces that span out of the supercells we used. We would need unrealistically large supercells to reach convergence [47]. For the particular case of bulk hexagonal Boron Nitride, while we were working on this project, Monserrat *et al.* presented a paper on arXiv

Supercell size	2	4	6	8	10
Gap corrections from :					
Thermal lines	-67.9	-97.1	-227	-221	-265
ZG displacement	-212	-323	-438	-272	-250
Thermal lines (phonons mapping)	-329	-350	-410	-370	-540
ZG displacement (phonons mapping)	-336	-251	-543	-189	-202

Table 3.1: *Corrections to the band gap with respect to the supercell size for polyethylene from different methods. The supercell size number is the number of repeated unit cells along the x axis. Gap corrections are given in meV.*

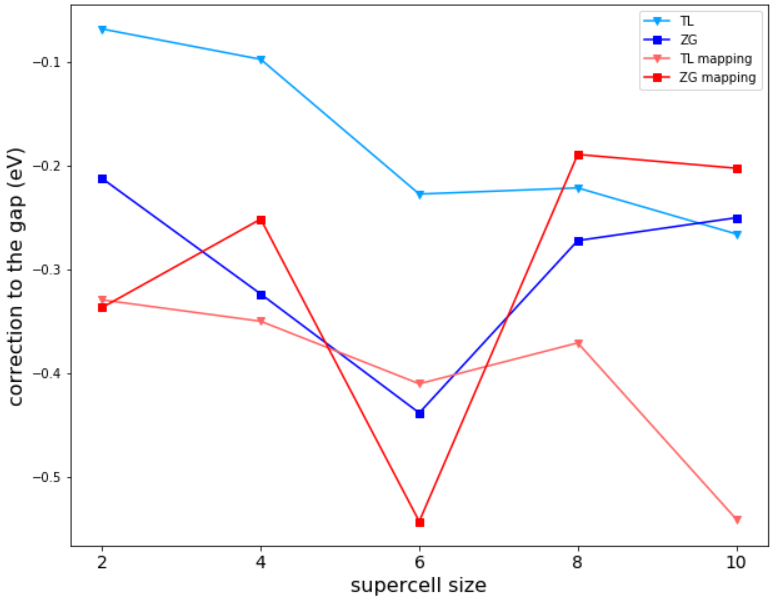

Figure 3.10: *Comparative plots of the gap correction of polytehtylene with respect to the supercell size, using four different methods.*

where they stated that we would need a 32x32x32 supercell to reach convergence [48], making it virtually impossible to compute in a reasonable time. The example of polyethylene is presented in figure 3.11. We used 50x1x1 **k**-point grid with a normconserving pseudopotential using a GGA exchange-correlation functional from the PseudoDojo project, setting the energy cutoff at 120 Rydberg. We see on the figure that convergence is not achieved in this range of supercell sizes.

For the Phosphorene however, as it is not polar, we managed to obtain a decent convergence. We used a 8x9x1 **k**-point grid and a similar pseudopotential from the PseudoDojo project, with an energy cutoff at 90 Rydberg. To increase the accuracy of the results, we averaged the gap corrections on two different ZG configurations. They are different only on the sign combination from equation 2.12. One of them has the alternating signs starting with a plus, the other one starts with a minus. In other words, the two different configurations differ by a -1 factor. This is a compromise between the thermal lines average and the ZG displacement. We also used rectangular supercells instead of square ones, which is supposed to accelerate the calculations [34]. The obtained curve is plotted in figure 3.12. For this particular material, the correction of the gap due to vibrational effects is already small in the bulk Black Phosphorus [20]. Our results show that it tends to zero in the

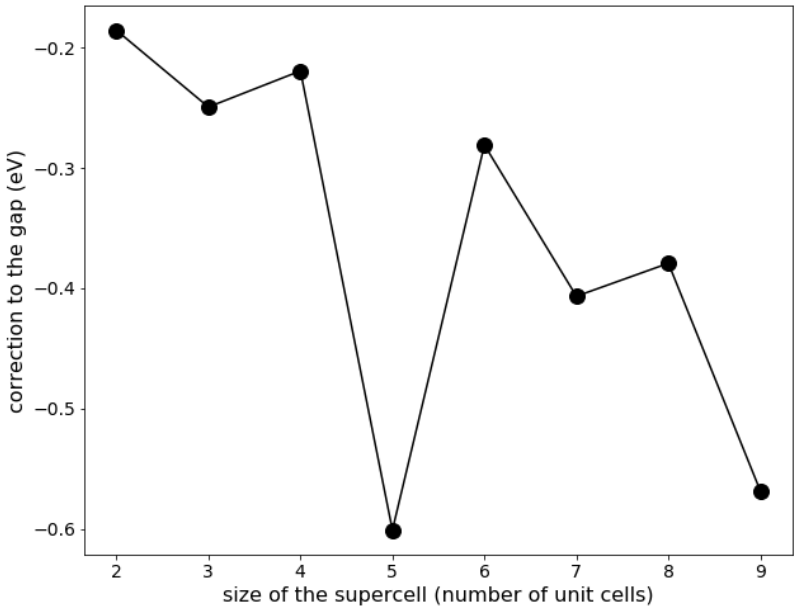

Figure 3.11: *Convergence of the gap corrections with respect to the supercell size for polyethylene, using the ZG displacement with mapped phonons. Supercell sizes indicate the number of repeated unit cells along the x axis.*

two-dimensional Phosphorene.

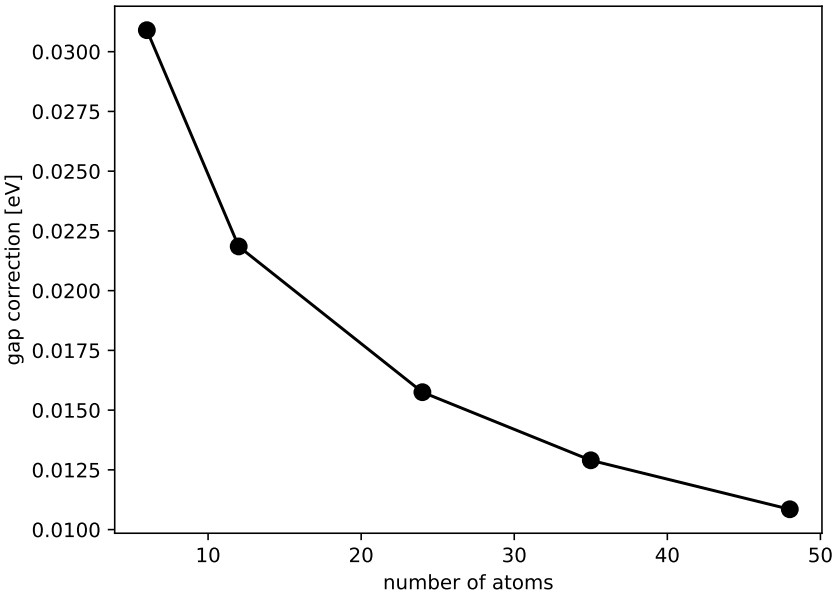

Figure 3.12: *Convergence of the gap corrections with respect to the number of atoms in the supercells for Phosphorene, using two ZG configurations with mapped phonons.*

Conclusion

At the beginning of this thesis we presented the theoretical framework, the density functional theory (DFT) in a plane wave formulation, in which we performed all the electronic calculations with the software Quantum ESPRESSO. Then we introduced the classical and quantum theory of phonons and the way we computed them, using density functional perturbation theory (DFPT). By using the DFPT results we show how to calculate the interaction between electrons and phonons, *via* the vibrational average. We derived a formula to compute this vibrational average for a generic electronic operator by the use of the mean-value theorem and the properties of the quantum harmonic oscillator's eigenstates. This formula is then applied to realistic systems with many vibrationals modes. In order to speed up calculations in large supercells, we introduce a mapping of phonons calculated in a unit cell at different q-points in the reciprocal space onto the central point of any chosen supercells. In this way, we have to perform only one DFPT calculation in a unit cell instead of multiple calculation in supercells of various sizes. This represents a great gain in computational time since the DFPT calculations in a plane waves formulation scale with the number of atoms in the simulation cell to the cube.

We presented two ways to compute the electron-phonon interaction by finite differences : the average on thermal lines proposed by B. Monserrat and a one-shot computation on a special configuration proposed by Zacharias and Giustino, that we call the ZG displacement.

The convergence of these two methods were tested on three different materials, for which we decided to look at the renormalization of the electronic gap due to electron-phonon interaction. The first material is polyethylene, a linear polymer. We picked it because the convergence on the gap correction with respect to the supercell size is supposed to be faster, since the polymer is one-dimensional. The second material is hexagonal Boron Nitride, a polar semi-conductor, for which the electron-phonon coupling is known to have an important role in its electronic and optical properties. The

third material is Phosphorene, a non polar semi-conductor with a wide electronic gap.

Although requiring a relatively low computational time, the results we obtained show that reaching convergence is difficult, especially for polar material for which huge supercell sizes are necessary. This is the case for polyethylene and hexagonal Boron Nitride. For non-polar materials, it seems possible to reach convergence but the electron-phonon coupling is small and the gap renormalization in case of phosphorene tends about to 0. On the methodology aspect, the average on thermal lines seems to give more accurate results and a smoother convergence than the ZG displacement. However an average on the ZG displacement and its opposite sign configuration seems a good compromise to reach convergence in a reasonable computational time.

In conclusion we found that reaching convergence of finite displacement with the supercell in polar materials is very difficult, and much more complicated than reported in the literature. On the other hand it is possible to achieve convergence of electron-phonon coupling properties in non-polar materials with a reasonable computational time. This open the possibility to apply these methods to other non-polar materials with a strong electron-phonon coupling such as diamond. Regarding the different methods tested in this thesis, we found that the best compromise is the average on two ZG configurations, that guarantees a smooth convergence with a small computational time.

For the future we plan to apply these methodologies in the study of other observable such as carrier transport or optical properties, that could converge faster than the electronic gap. This will give as the possibility to investigate the anomalous behaviors of optical excitations with temperature reported in different experimental measurements. Finally we would like to compare our results with the ones obtained by the perturbative approach, and see the role of the different approximations in the two methods.

Bibliography

[1] PB Allen and M Cardona. Temperature dependence of the direct gap of si and ge. *Physical review B*, 27(8):4760, 1983.

[2] Philip B Allen and Volker Heine. Theory of the temperature dependence of electronic band structures. *Journal of Physics C: Solid State Physics*, 9(12):2305, 1976.

[3] Elena Cannuccia and Andrea Marini. Effect of the quantum zero-point atomic motion on the optical and electronic properties of diamond and trans-polyacetylene. *Physical review letters*, 107(25):255501, 2011.

[4] Gabriel Antonius, Samuel Poncé, E Lantagne-Hurtubise, Gabriel Auclair, Xavier Gonze, and Michel Côté. Dynamical and anharmonic effects on the electron-phonon coupling and the zero-point renormalization of the electronic structure. *Physical Review B*, 92(8):085137, 2015.

[5] Kristen Kaasbjerg, Kristian S Thygesen, and Karsten W Jacobsen. Phonon-limited mobility in n-type single-layer mos 2 from first principles. *Physical Review B*, 85(11):115317, 2012.

[6] Samuel Poncé, Elena R Margine, Carla Verdi, and Feliciano Giustino. Epw: Electron–phonon coupling, transport and superconducting properties using maximally localized wannier functions. *Computer Physics Communications*, 209:116–133, 2016.

[7] Feliciano Giustino. Electron-phonon interactions from first principles. *Reviews of Modern Physics*, 89(1):015003, 2017.

[8] Bartomeu Monserrat. Vibrational averages along thermal lines. *Phys. Rev. B*, 93:014302, Jan 2016.

[9] Marios Zacharias and Feliciano Giustino. One-shot calculation of temperature-dependent optical spectra and phonon-induced band-gap renormalization. *Phys. Rev. B*, 94:075125, Aug 2016.

[10] Marios Zacharias and Feliciano Giustino. Theory of the special displacement method for electronic structure calculations at finite temperature. *Physical Review Research*, 2(1):013357, 2020.

[11] Rafael Ramírez, Carlos P Herrero, Eduardo R Hernández, and Manuel Cardona. Path-integral molecular dynamics simulation of 3 c- si c. *Physical Review B*, 77(4):045210, 2008.

[12] Bartomeu Monserrat and David Vanderbilt. Temperature effects in the band structure of topological insulators. *Physical Review Letters*, 117(22):226801, 2016.

[13] Jean-Nicolas Dumez and Chris J Pickard. Calculation of nmr chemical shifts in organic solids: Accounting for motional effects. *The Journal of chemical physics*, 130(10):104701, 2009.

[14] Ferenc Karsai, Moritz Humer, Espen Flage-Larsen, Peter Blaha, and Georg Kresse. Effects of electron-phonon coupling on absorption spectrum: K edge of hexagonal boron nitride. *Physical Review B*, 98(23):235205, 2018.

[15] Carina Faber, Paul Boulanger, Claudio Attaccalite, Elena Cannuccia, Ivan Duchemin, Thierry Deutsch, and Xavier Blase. Exploring approximations to the g w self-energy ionic gradients. *Physical Review B*, 91(15):155109, 2015.

[16] Bartomeu Monserrat. Correlation effects on electron-phonon coupling in semiconductors: Many-body theory along thermal lines. *Physical Review B*, 93(10):100301, 2016.

[17] Carina Faber, Ivan Duchemin, Thierry Deutsch, Claudio Attaccalite, Valerio Olevano, and Xavier Blase. Electron–phonon coupling and charge-transfer excitations in organic systems from many-body perturbation theory. *Journal of Materials Science*, 47(21):7472–7481, 2012.

[18] Yatendra Pal Varshni. Temperature dependence of the energy gap in semiconductors. *physica*, 34(1):149–154, 1967.

[19] A Surrente, AA Mitioglu, K Galkowski, W Tabis, DK Maude, and P Plochocka. Excitons in atomically thin black phosphorus. *Physical Review B*, 93(12):121405, 2016.

[20] Cesar EP Villegas, AR Rocha, and Andrea Marini. Anomalous temperature dependence of the band gap in black phosphorus. *Nano letters*, 16(8):5095–5101, 2016.

[21] Neil W Ashcroft, N David Mermin, et al. Solid state physics [by] neil w. ashcroft [and] n. david mermin., 1976.

[22] Charles Kittel, Paul McEuen, and Paul McEuen. *Introduction to solid state physics*, volume 8. Wiley New York, 1996.

[23] Pierre Hohenberg and Walter Kohn. Inhomogeneous electron gas. *Physical review*, 136(3B):B864, 1964.

[24] Walter Kohn and Lu Jeu Sham. Self-consistent equations including exchange and correlation effects. *Physical review*, 140(4A):A1133, 1965.

[25] Paul AM Dirac. Note on exchange phenomena in the thomas atom. In *Mathematical Proceedings of the Cambridge Philosophical Society*, volume 26, pages 376–385. Cambridge University Press, 1930.

[26] David M Ceperley and Berni J Alder. Ground state of the electron gas by a stochastic method. *Physical Review Letters*, 45(7):566, 1980.

[27] John P Perdew. Accurate density functional for the energy: Real-space cutoff of the gradient expansion for the exchange hole. *Physical Review Letters*, 55(16):1665, 1985.

[28] John P Perdew, Kieron Burke, and Matthias Ernzerhof. Generalized gradient approximation made simple. *Physical review letters*, 77(18):3865, 1996.

[29] Paolo Giannozzi, Stefano Baroni, Nicola Bonini, Matteo Calandra, Roberto Car, Carlo Cavazzoni, Davide Ceresoli, Guido L Chiarotti, Matteo Cococcioni, Ismaila Dabo, Andrea Dal Corso, Stefano de Gironcoli, Stefano Fabris, Guido Fratesi, Ralph Gebauer, Uwe Gerstmann, Christos Gougoussis, Anton Kokalj, Michele Lazzeri, Layla Martin-Samos, Nicola Marzari, Francesco Mauri, Riccardo Mazzarello, Stefano Paolini, Alfredo Pasquarello, Lorenzo Paulatto, Carlo Sbraccia, Sandro Scandolo, Gabriele Sclauzero, Ari P Seitsonen, Alexander Smogunov, Paolo Umari, and Renata M Wentzcovitch. Quantum espresso: a modular and open-source software project for quantum simulations of materials. *Journal of Physics: Condensed Matter*, 21(39):395502 (19pp), 2009.

[30] Paolo Giannozzi, Oscar Baseggio, Pietro Bonfà, Davide Brunato, Roberto Car, Ivan Carnimeo, Carlo Cavazzoni, Stefano de Gironcoli, Pietro Delugas, Fabrizio Ferrari Ruffino, Andrea Ferretti, Nicola Marzari, Iurii Timrov, Andrea Urru, and Stefano Baroni. Quantum espresso toward the exascale. *The Journal of Chemical Physics*, 152(15):154105, 2020.

[31] P Giannozzi, O Andreussi, T Brumme, O Bunau, M Buongiorno Nardelli, M Calandra, R Car, C Cavazzoni, D Ceresoli, M Cococcioni, N Colonna, I Carnimeo, A Dal Corso, S de Gironcoli, P Delugas, R A DiStasio Jr, A Ferretti, A Floris, G Fratesi, G Fugallo, R Gebauer, U Gerstmann, F Giustino, T Gorni, J Jia, M Kawamura, H-Y Ko, A Kokalj, E Küçükbenli, M Lazzeri, M Marsili, N Marzari, F Mauri, N L Nguyen, H-V Nguyen, A Otero de-la Roza, L Paulatto, S Poncé, D Rocca, R Sabatini, B Santra, M Schlipf, A P Seitsonen, A Smogunov, I Timrov, T Thonhauser, P Umari, N Vast, X Wu, and S Baroni. Advanced capabilities for materials modelling with quantum espresso. *Journal of Physics: Condensed Matter*, 29(46):465901, 2017.

[32] Felix Bloch. Über die quantenmechanik der elektronen in kristallgittern. *Zeitschrift für physik*, 52(7-8):555–600, 1929.

[33] Hendrik J Monkhorst and James D Pack. Special points for brillouin-zone integrations. *Physical review B*, 13(12):5188, 1976.

[34] Bartomeu Monserrat. Electron–phonon coupling from finite differences. *Journal of Physics: Condensed Matter*, 30(8):083001, feb 2018.

[35] MJ Van Setten, Matteo Giantomassi, Eric Bousquet, Matthieu J Verstraete, Don R Hamann, Xavier Gonze, and G-M Rignanese. The pseudodojo: Training and grading a 85 element optimized norm-conserving pseudopotential table. *Computer Physics Communications*, 226:39–54, 2018.

[36] Nicholas A Lanzillo and Curt M Breneman. Band gap engineering in polymers through chemical doping and applied mechanical strain. *Journal of Physics: Condensed Matter*, 28(32):325502, 2016.

[37] Xinjiang Wang, Massoud Kaviany, and Baoling Huang. Phonon coupling and transport in individual polyethylene chains: a comparison study with the bulk crystal. *Nanoscale*, 9(45):18022–18031, 2017.

[38] Guillaume Cassabois, Pierre Valvin, and Bernard Gil. Hexagonal boron nitride is an indirect bandgap semiconductor. *Nature Photonics*, 10(4):262–266, 2016.

[39] Xavier Blase, Angel Rubio, Steven G Louie, and Marvin L Cohen. Quasiparticle band structure of bulk hexagonal boron nitride and related systems. *Physical review B*, 51(11):6868, 1995.

[40] B Arnaud, S Lebègue, P Rabiller, and M Alouani. Huge excitonic effects in layered hexagonal boron nitride. *Physical review letters*, 96(2):026402, 2006.

[41] Kenji Watanabe, Takashi Taniguchi, and Hisao Kanda. Direct-bandgap properties and evidence for ultraviolet lasing of hexagonal boron nitride single crystal. *Nature materials*, 3(6):404–409, 2004.

[42] Elena Cannuccia, B Monserrat, and Claudio Attaccalite. Theory of phonon-assisted luminescence in solids: application to hexagonal boron nitride. *Physical Review B*, 99(8):081109, 2019.

[43] Mehran Amiri, Javad Beheshtian, Farzaneh Shayeganfar, Mahdi Faghihnasiri, Rouzbeh Shahsavari, et al. Electro-optical properties of monolayer and bilayer pentagonal bn: First principles study. *Nanomaterials*, 10(3):440, 2020.

[44] Han Liu, Adam T Neal, Zhen Zhu, David Tomanek, and Peide D Ye. Phosphorene: a new 2d material with high carrier mobility. *arXiv preprint arXiv:1401.4133*, 2014.

[45] Zhinan Guo, Han Zhang, Shunbin Lu, Zhiteng Wang, Siying Tang, Jundong Shao, Zhengbo Sun, Hanhan Xie, Huaiyu Wang, Xue-Feng Yu, et al. From black phosphorus to phosphorene: basic solvent exfoliation, evolution of raman scattering, and applications to ultrafast photonics. *Advanced Functional Materials*, 25(45):6996–7002, 2015.

[46] Baisheng Sa, Yan-Ling Li, Zhimei Sun, Jingshan Qi, Cuilian Wen, and Bo Wu. The electronic origin of shear-induced direct to indirect gap transition and anisotropy diminution in phosphorene. *Nanotechnology*, 26(21):215205, 2015.

[47] A Pishtshev and N Kristoffel. Understanding the electron-phonon interaction in polar crystals: Perspective presented by the vibronic theory. In *Journal of Physics. Conference Series (Online)*, volume 833, 2017.

[48] Ryan James Hunt, Bartomeu Monserrat, Viktor Zólyomi, and ND Drummond. Diffusion quantum monte carlo and g w study of the electronic properties of monolayer and bulk hexagonal boron nitride. *Physical Review B*, 101(20):205115, 2020.